Sanja Asikainen

LOAD-BEARING BIOACTIVE HYBRID MATERIALS

School of Electrical Engineering

Thesis submitted for examination for the degree of Master of Science in Technology in Espoo, 28.1.2013.

Supervisor:

Professor Jukka Seppälä

Instructor:

Minna Malin, Lis.Sc. (Tech)

Author

Sanja Asikainen

Title

Load-bearing bioactive hybrid materials

Abstract

The aim of this thesis was to study the preparation of three dimensional load-bearing bioactive hybrid materials for orthopedic applications. The application area is interbody cage in spinal fusion. The load-bearing component in the material is electron beam melting (EBM) manufactured titanium alloy ($TiAl_6V_4$) mesh, whereas the bioactive component was either crushed bone graft or composite made of biodegradable polymer and bioactive glass (BAG). Polymers were made porous to allow bone ingrowth.

In this study, porous structures were made of thermoplastic and photocrosslinkable polycaprolactone (PCL). Three methods were used to prepare porous structures of thermoplastic PCL: freeze drying, freeze extraction and dipping. Porous structure of freeze extraction samples was determined using micro computed tomography (μCT) and scanning electron microscope. Pores were interconnected and porosity was 66-76 %. However, the pore size was probably too small for cell ingrowth. For photocorsslinking of PCL, methacrylated PCL oligomer was synthetized and mixed with BAG and porogen agent salt. Titanium alloy mesh was immersed in the mixture and the polymer was photocrosslinked.

Compression strength at break was determined for photocrosslinked samples and trabecular bone samples. Compression strength at break (8 MPa) and compressive modulus (0.2 GPa) for titanium meshes were close to literature values of trabecular bone (2-22 MPa and 0.2-1.9 GPa, respectively). Therefore, the hybrid material is probably suitable for interbody cage fusion, because vertebrae are trabecular bone. However, cortical bone has much higher compression strength values at literature (100-230 MPa). Therefore the materials cannot be used in cortical bone applications.

Supervisor	Instructor
Professor Jukka Seppälä	Minna Malin, Lic.Sc. (Tech.)
Chair	Chair code
Polymer technology	Kem-100
Pages	Language
8 + 84	English
Keywords	Date
TiAl6V4, electron beam melting, scaffolds, spinal fusion, orthopedics	28.1.2013

AALTO-YLIOPISTO DIPLOMITYÖN TIIVISTELMÄ

SÄHKÖTEKNIIKAN KORKEAKOULU

Tekijä

Sanja Asikainen

Diplomityön nimi

Load-bearing bioactive hybrid materials

Tiivistelmä

Diplomityön tavoitteena oli tutkia kolmiulotteisten kuormaa kantavien bioaktiivisten hybridimateriaalien valmistusta ortopedisiin sovelluksiin. Sovelluskohteeksi valittiin välilevyimplantti spinaalifuusioon. Kuormaa kantavana komponenttina materiaalissa toimi EBM -menetelmällä valmistettu titaaniseosverkko ($TiAl_6V_4$), kun taas bioaktiivisena komponenttina toimi joko pankkiluumurska tai biohajoavan polymeerin ja bioaktiivisen lasin muodostama komposiitti. Polymeeri huokoistettiin solujen sisään kasvun mahdollistamiseksi.

Tutkimuksessa valmistettiin huokoisia polymeerirakenteita termoplastisesta sekä valosilloittuvasta poly(ε-kaprolaktonista). Termoplastisesta polymeeristä valmistettiin huokoisia rakenteita kolmella eri tavalla: kylmäkuivaamalla, kylmäuutolla sekä kastamismenetelmällä. Kylmäuutetuiden näytteiden huokoisuusrakenne selvitettiin µCT-kuvantamisella sekä pyyhkäisyelektronimikroskoopilla, jolloin selvisi, että huokoisuus on yhtenäistä ja huokoisuus oli 66-76 %. Huokoskoko on kuitenkin todennäköisesti liian pieni solujen sisään kasvulle. Polymeerin valosilloitusta varten syntetisoitiin metakryloitua ε-kaprolaktoni oligomeeriä, minkä jälkeen se sekoitettiin bioaktiivisen lasin sekä huokoisuuden aikaan saavan suolan kanssa. Titaaniverkko upotettiin massaan ja polymeeri valosilloitettiin.

Työssä määritettiin valosilloitettujen polymeerinäytteiden sekä hohkaluunäytteiden puristuslujuus. Titaaniseosverkkojen puristuslujuus (8 MPa) sekä puristusmoduuli (0.2 GPa) olivat samaa suuruusluokkaa hohkaluun kirjallisuusarvojen kanssa (2-22 MPa ja 0.2-1.9 GPa). Puristuslujuusarvojen perusteella hybridimateriaali on mahdollisesti sopiva haluttuun sovelluskohteeseen selkärangassa, jossa on hohkaluuta. Kortikaaliluun sovelluksiin materiaali ei kuitenkaan sovellu, sillä kortikaaliluulla on huomattavasti korkeammat puristuslujuuden arvot kirjallisuudessa (100-230 MPa).

Työn valvoja Professori Jukka Seppälä	Ohjaaja Minna Malin, TkL
Professuuri Polymeeriteknologia	Professuurin koodi Kem-100
Sivumäärä 8 + 84	Kieli Englanti
Avainsanat $TiAl_6V_4$, kudosteknologian tukirakenteet, spinaalifuusio, 3D-pikavalmistus, ortopedia	Päivämäärä 28.1.2013

Acknowledgements

The work behind this thesis was undertaken at Aalto University in the School of Chemical Technology and the Department of Biotechnology and Chemical Technology between June, 2012 and January, 2013.

First of all, I would like to thank Professor Jukka Seppälä for both providing the opportunity to for this thesis and for his supervision. I warmly thank my instructor Minna Malin for her guidance and valuable feedback on my thesis. In addition, I want to express my gratefulness to Professor Petri Lehenkari (Institute of Biomedicine, University of Oulu) for providing the bone samples and also fruitful ideas for this study.

I would like to acknowledge Mikko Finnilä (Institute of Biomedicine, University of Oulu) for the μCT images and Eero Huotilainen (Business, Innovation, Technology unit, Aalto University) for the titanium networks. I want to thank the whole personnel at the polymer technology laboratory for their advices: especially Luong Nguyen for carrying out the SEM imaging, Jaana Rich for assisting the mechanical testing and Harri Korhonen and Laura Elomaa for the practical advice.

Finally, I warmly thank my dear family and friends. Special thanks goes to Venla for discussions and encouragement and Joni for his support.

Otaniemi, Espoo, 28.1.2013

Sanja Asikainen

Contents

Symbols and abbreviations

EBM	Electron beam melting
ESEM	Environmental scanning electron microscopy
EDX	Energy dispersive x-ray spectroscopy
3D	Three dimensional
ALIF	Anterior lumbar interbody fusion
AM	Laser additive manufacturing
BAG	Bioactive glass
BMP-2	Bone morphogenetic protein 2
$Ca(OH)_2$	Calcium hydroxide
$CaCO_3$	Calcium carbonate
CAD	Computer-aided design
CAM	Computer-aided manufacturing
CBCT	Cone beam computed tomography
CL	E-caprolactone
Co-Cr	Cobalt-chrome
CP	Commercially pure
CQ	Camphorquinone
DDD	Degenerative disc disease
EDX	Energy dispersive x-ray spectroscopy
ELI	Extra low interstitial
FDA	U.S. food and drug administration
HA	Hydroxyapatite
HBSS	Hank’s balanced salt solution
HDPE	High-density-polyethylene
LMD	Laser metal deposition
LM	Laser melting
LS	Laser sintering
MAAH	Methacrylic anhydride
Mn	Number average molecular weight
NMR	Nuclear magnetic resonance
PCL	Polycaprolactone
PDI	Polydispersity index
PEEK	Polyetheretherketone

PERYT	Pentaerythritol
PET	Polyethylene terephthalate
PLIF	Posterior lumbar interbody fusion
PLLA	Poly-L-lactide
PMMA	Polymethylmetacrylate
PU	Polyurethane
RP	Rapid prototyping
SEC	Size-exclusion chromatography
SEM	Scanning electron microscopy
$Sn(Oct)_2$	Stannous(ii)2-ethylhexanoate
TDR	Total disc replacement
Ti	Titanium
Ti64	$TiAl_6V_4$
TLIF	Transforaminal lumbar interbody fusion
UHMWPE	Ultra-high-molecular-weight polyethylene
XDR	X-ray diffraction
β-TCP	Tricalcium phosphate
µCT	Micro-computed tomography

1 Introduction

The history of load-bearing implants is long. However, the ancient orthopedic procedures generally resulted in amputation rather than repair. The first steps in the development of orthopedic implants were introduced in the late 19th century. One of the most important aspects was the development of antiseptic surgical techniques. Early hip arthoplasty and its development have been the foundation for implants in general. Numerous failures have provided the groundwork for better understanding of concepts such as biocompatibility, behavior of materials in body and functionality of the musculoskeletal system. [1]

Life expectancy of the human being has risen considerably during the last century. The aging of the population increases the number of people suffering from degenerative diseases. Degenerative diseases effect on human joints and can lead to pain and loss in function. A significant proportion of population over the age 40 suffers from these kinds of degenerative diseases. Musculoskeletal disorders are the most widespread human health problem. A normal self-healing process cannot repair effects of degenerative diseases. Therefore, there is a need for long lasting orthopedic implants, which restore the function or remove the pain. [2]

The primary target of this thesis was to study the possibility to prepare three-dimensional (3D) bioactive hybrid materials consisting of titanium mesh and biodegradable polymer. The planned application area is orthopedic implants. The role of titanium is to function as a load-bearing component, whereas the polymer matrix offers suitable porous structure for cell-ingrowth. The biodegradable polymer matrix includes bioactive glass to induce cell growth. Titanium alloy meshes were manufactured by electron beam melting (EBM). The big advantage of this method is the possibility to manufacture 3D components according to the model with high accuracy. During the work, the use of bone graft as a filler in titanium mesh was also investigated.

This thesis consists of a literature part and an experimental part. The literature part includes an overview of the properties and structure of bone. Requirements for biomaterials in orthopedics are presented. The role of titanium as implant material is introduced and different methods to manufacture porous titanium are described. The target of this study was to prepare titanium/polymer hybrid materials. Therefore, recent methods used to prepare polymer/titanium hybrid materials are presented.

Since the EBM method was used in the experimental part, it is discussed more widely in the literature part. Finally, the literature part focuses on the anatomy of spine and spinal implants because it is the planned application area.

In the experimental part, two different biodegradable polymers are used. The first is photo-crosslinkable polycaprolactone (PCL) and the second is thermoplastic polycaprolactone. Firstly, four-branched PCL oligomers were synthesized. Oligomers were methacrylated to receive a photo-crosslinkable oligomer. These oligomers were blended with bioactive glass and salt after which EBM manufactured titanium mesh was filled with mixture. The mixture was cross-linked, salt was leached to receive a porous structure and compression testing was performed. Secondly, thermoplastic PCL was used and other methods to prepare porous polymer structure were tested: freeze-extraction, freeze drying and dipping. Freeze-extraction samples were characterized using scanning electron microscopy (SEM) and micro-computed tomography (μCT) visualizations.

In addition to biodegradable polymers, also bone graft was used. Titanium mesh was filled with crushed bone graft and imaged with μCT and cone beam computed tomography (CBCT). Titanium mesh filled with bone as well as two samples of trabecular bone were compression tested. The obtained compression test results were compared with literature values for bone and EBM manufactured titanium mesh.

LITERATURE PART

2 Properties and structure of bone

Bone tissue makes up to 18 % of the weight of the human body. Bone tissue belongs to the group of connective tissues and has several important functions. First, it supports soft tissue and protects internal organs. Second, it provides an attachment for tendons of most skeletal muscles and assists in movement along with skeletal muscles. Third, it stores and releases minerals, especially calcium and phosphorus, maintaining critical mineral balances. Furthermore, red bone marrow in certain bones produces red blood cells, white blood cells and platelets. Finally, it also contains yellow bone marrow, which stores triglycerides and functions as a chemical energy reserve. [3]

2.1 Structure of bone

The skeletal system can be divided into trabecular bone and cortical bone by the structure. Trabecular bone has a sponge-like trabecular structure that occupies the inner region of the epiphysis and metaphysis whereas cortical bone is a semi-solid shell that covers the bone. [4] Trabecular bone is also called cancellous or spongy bone. [5] Cortical bone has biomechanical, supportive and protective properties. [4] Figure 1 shows the anatomy of long bone. Long bones such as the femur or tibia have two epiphyses and one diaphysis. Epiphyses are made of trabecular bone covered by a shell of cortical bone. Diaphysis is composed primarily of cortical bone. [1]

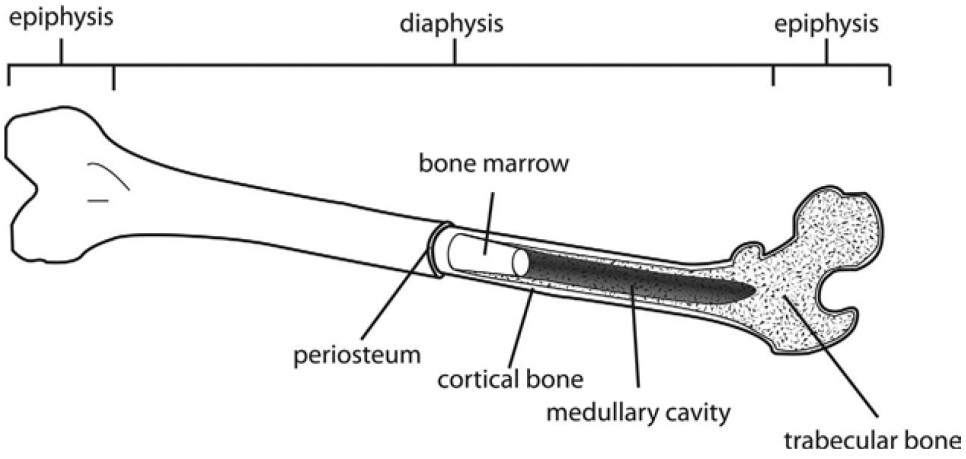

Figure 1. Anatomy of a long bone. [1]

Cortical bone is the main tissue type of the skeletal system. Up to 80 % of the entire adult skeletal mass consists of cortical bone and only 20 % consists of trabecular bone. The surface area of cortical bone is relatively small, 33 % of the total bone surface, and the surface to volume ratio is 2.5. [4]

Cortical bone is porous. The porosity is due to Haversian canals, Volkmann's canals and resorption cavities. The pores contain primarily nervous tissue and blood vessels. The Haversian canals are nearly parallel with the major axis of bone and are interconnected by Volkmann's canals. The Volkmann's canals are oriented perpendicular to the skeletal loading axis. The canals form a three-dimensional network throughout the cortical bone. Inside this network, there are circulatory vessels and nerves. The network functions also as extracellular fluid path allowing the exchange of nutrition, nerve signals, and metabolites between bone and other tissues. [4] The porosity of cortical bone that is due to the Haversian and Volkmann's canals ranges from 5 - 30 % [1].

Osteons are cylindrical conformations and comprised of individual sheets of mineralized tissue (lamellae). A diameter of an osteon is 200-250 μm and thickness of a lamella is 1-5 μm. Each osteon contains approximately 20 - 30 lamellae that wrap around the Haversian canal. Lacunae are ellipsoidal, 5 - 8 μm long pores containing osteocytes. The lacunae are interconnected by channels called canaliculi (approximately 0.5 μm in diameter). The organization of cortical bone is illustrated in Figure 2. [1]

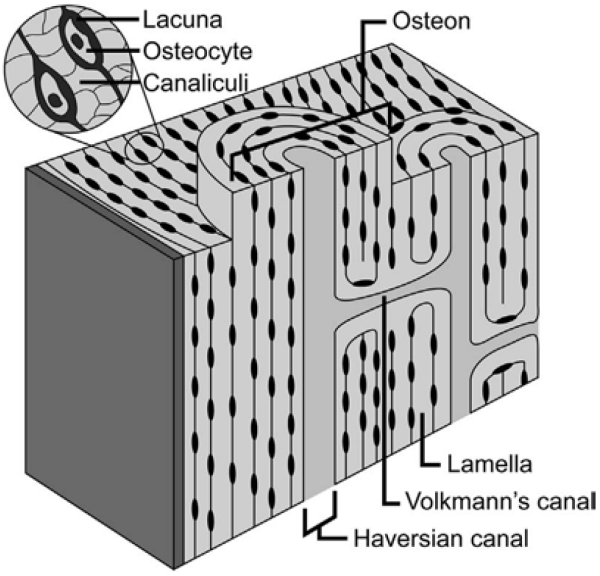

Figure 2. The organization of cortical bone into osteons. [1]

Cortical bone is constantly renewing in response to environmental signals and microdamage. The complex process of renewal is called remodeling. During this process pre-existing osteons are partially removed to make space for newly generated osteons. [4]

The surface area of trabecular bone is larger when compared to that of cortical bone. The surface to volume ratio is approximately 20. Trabecular bone is composed of a large number of a rod or plate shaped trabeculae (Figure 3). Trabeculae form a sponge-like network. [4] The network is open three-dimensional interconnected structure. [1]

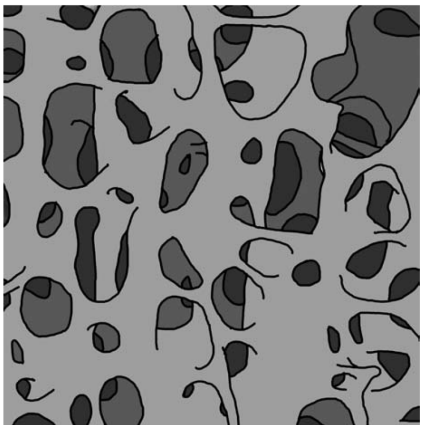

Figure 3. Illustration of the network structure of trabecular bone, showing both sheet-like (plate) and thin and beam-like (rod) morphologies. [1]

A cellular structure of trabecular bone is significantly less stiff in comparison with that of cortical bone. It is more isotropic at its macrostructure level although it is heterogeneous at the microstructure level. The structure of trabecular bone can be dramatically different depending on the anatomical site investigated and the health, age and an activity level of the individual. The trabecular bone porosity can range from 30 % to 90 %. The highest porosities are associated with elderly vertebrae. Figure 4 illustrates the structure of trabecular bone. [1]

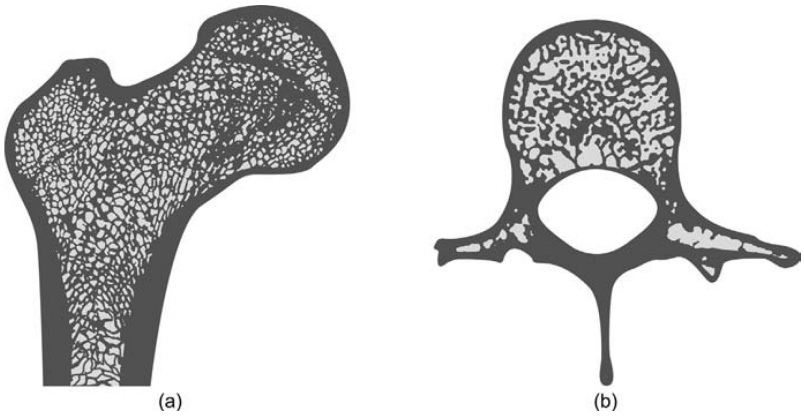

Figure 4. Schematic of trabecular bone structure in (a) the proximal femur and (b) vertebral body. [1]

The proportions of trabecular and cortical tissues vary significantly depending on bone. The proportion of cortical bone of total bone in an ulna can be 92 %, whereas it is 62 % in a typical vertebra. [4]

2.2 Composition of bone

Bone consists of an organic matrix (20-40 %), inorganic minerals (50-70 %), cellular elements (5-10 %), and lipids (3 %). The organic bone matrix is mostly collagen molecules that are bundled together to form collagen fibers. Collagen fibers are aligned parallel to each other to form a lamella sheet. Hydroxyapatite (HA) is the predominant molecule of a bone mineral and is deposited in the gap regions of collagen fibers. [4] HA ($Ca_{10}(PO_4)_6(OH)_2$) is formed when calcium phosphate ($Ca_3(PO_4)_2$) combines with calcium hydroxide ($Ca(OH)_2$) [3]. HA exists in the form of needle-, plate- or rod-shaped crystals and it provides the bone matrix with

mechanical rigidity and load-bearing capacity. HA contains a lot of impurities that are either incorporated into the crystal lattice or absorbed onto the crystal surface. These impurities are mineral salts such as calcium carbonate ($CaCO_3$), and ions such as magnesium, fluoride, potassium, and sulfate [3]. Impurities influence the solubility of the crystal and for that reason the HA in bone is more soluble than geologic apatite. [4]

The major cellular elements of bone include osteoclasts, osteoblasts, osteocytes, bone-lining cells, along with the precursors of these specialized cells, and cells of the marrow compartment and the immune regulatory system. [4] Osteogenic cells are unspecialized stem cells. They are derived from mesenchyme where almost all connective tissues are formed. [3]

The osteoclasts are bone resorbing cells with a diameter ranging from 20 to over 200 microns. Osteoclasts may live for up to seven weeks, but the nucleus lives up to 10 days. At the end of their lifespan osteoclasts migrate into adjacent marrow space and undergo apoptosis. [4] Apoptosis is a programmed cell death, which is a normal type of cell death. During apoptosis, the cell ceases its functions and in the end phagocytes engulf and digest the cell. [3] The osteoblasts are bone-forming cells that synthesize and secrete collagen to form an unmineralized bone matrix. Typically, osteoblasts are 15-30 microns cuboidal-shaped cells and they are activated by specific mechanical and nonmechanical stimuli. Active osteoblasts are transformed to bone-lining cells, osteocytes, or they undergo apoptosis. [4]

The bone-lining cells are also known as resting osteoblasts because they are derived from the surface of osteoblasts. The bone-lining cells are interconnected as a cellular sheet that covers the bone surfaces. They are flat and elongated, about 1 micron thick and 12 microns by their diameter. They serve as a barrier to protect the bone surfaces from inappropriate resorption by osteoclasts, other inflammatory cells and ions. The bone-lining cells may have a role in maintaining a suitable microenvironment for the growth of bone crystals. The bone-lining cell density decreases with age. [4]

Osteocyte is the main bone cell type in mature bone. About 95 % of total bone cells are osteocytes. The cell size and organelles reduce as the osteocyte ages. The lifespan of an osteocyte depends on the rate of bone turnover because osteocytes are removed during bone formation. Most of the osteocytes eventually undergo

apoptosis. The rate of apoptosis and bone loss are increased for example by aging, unloading and loss of estrogen. Overall, the total bone mass decreases 1 % per year. [4]

2.3 Mechanical properties of bone

The architecture of bone is complex and the properties of bone tissue vary remarkably. Porosity, pore size, mineralization and mineral density, cell type and a cytokines gradient feature affect the properties of the bone tissue. [6] The density of wet bone is 1990 g/cm^3 [7].

The hardness of bone depends on the crystallized inorganic salts whereas the bone's flexibility depends on its collagen fibers. [3,8] Collagen fibers and other organic molecules act as reinforcing components providing tensile strength. If mineral salts are removed from bone, the bone becomes rubbery and flexible. [3] The behavior of bone is similar to that of relatively brittle polymer composite material [8].

The mechanical properties of bone depend on age. After maturation, the tensile strength and modulus of elasticity of femoral cortical bone decline by approximately 2 % per decade. [6] The biological variability often dominates the results of mechanical testing. In addition to age, activity levels and health conditions also gender, the stages of bone modeling and remodeling, mechanical or drug interventions, and bone metabolic disorders etc. affect the mechanical properties. A degree of mineralization and hardness or stiffness of the bone matrix may vary according to a site and a region. Accordingly, the part or origin of the bone must be specified. Also the direction in which the specimen is tested is important because the bone is anisotropic and the mechanical properties are direction-dependent. [4] The strain rate affects the mechanical testing results. Higher strain rates generally produce a higher modulus of elasticity, a higher strength, and a greater strain to failure when compared to specimens tested at lower strain rate. [7]

Bone properties are not based on linear elasticity and the typical force-deformation curve is divided into four regions: toe (preloading) region, linear elastic region, non-linear elastic (plastic, micro-failure) region, and failure region (Figure 5). [4]

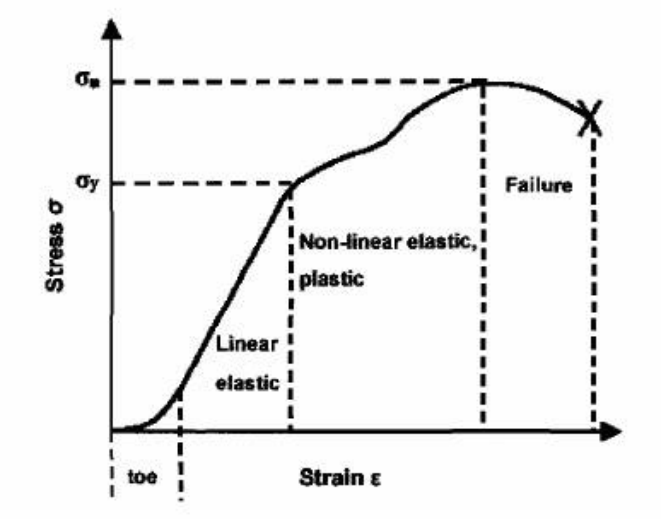

Figure 5. A typical stress-strain curve showing the nonlinearity, often seen in indentation test of trabecular bone. [4]

The testing environment may also influence the mechanical behavior of bone. The temperature, humidity, moisture and dryness are affecting factors in the environment. The physiological temperature is 37 °C. Testing at the room temperature 23 °C increases the Young's modulus of bone about 2-4 % when compared to testing at the physiological temperature. The moisture of the specimen should be kept constant with physiological saline. If the bone specimen dries, it will become more brittle and it's Young's modulus and strength will generally increase and its toughness will decrease. Therefore testing should be conducted in 0.9 % saline at a controlled temperature of 37 °C. [4] Also drying the bone and re-wetting it produces small differences in mechanical behavior [7].

The values for mechanical properties differ depending on a source. The values have a great range due to different treatment of specimens, age and health of donors and differences in sites of bones. The compressive and tensile moduli are similar. Tests for femoral specimens have also shown that there is no significant difference between the moduli at the 95 % confidence level [7]. Young's modulus of the human bone is typically 10 – 30 GPa [9-11]. The values for mechanical properties of cortical and trabecular bone are summarized in Table 1.

Table 1. Mechanical properties of cortical bone and trabecular bone.

Bone type	Compressive strenght (MPa)	Tensile Strenght (MPa)	Compression: Modulus of elasticity (GPa)	Tension: Modulus of elasticity (GPa)	Source
Cortical bone	100 - 230				[5]
Cortical bone, longitudinally	170 - 190	120 -130		17	[1]
	205	133			[7]
	195	133	17.4	17.4	[9]
	193	133	17	17	[8]
Cortical bone, transversely	133	51		11.5	[1]
	33	51	11.5	11.5	[8]
	130	52			[7]
	133	51	9.6	9.6	[9]
Trabecular bone	2 - 12				[5]
	7 - 22		0.2 - 1.9		[12]

Table 2 shows mechanical properties for different bone tissues. Long bones (arm and leg bones) have rather similar mechanical properties whereas vertebrae have remarkably lower values.

Table 2. Mechanical properties of bone tissues. [13]

Tissue	Direction of test	Modulus of elasticity (GPa)	Tensile strenght (MPa)	Compressive strength (MPa)
Leg bones				
Femur	Longitudinal	17.2	121	167
Tibia	Longitudinal	18.1	140	159
Fibula	Longitudinal	18.6	146	123
Arm bones				
Humerus	Longitudinal	17.2	130	132
Radius	Longitudinal	18.6	149	114
Ulna	Longitudinal	18.0	148	117
Vertebrae				
Cervical	Longitudinal	0.23	3.1	10
Lumbar	Longitudinal	0.16	3.7	5
Spongy bone	Longitudinal	0.09	1.2	1.9
Skull	Tangential	-	25	-
	Radial	-	-	97

3 Three-dimensional biomaterials in orthopedics

The definition of a biomaterial has undergone changes during the evolution of materials science. At first, in 1987, a biomaterial was defined as a non-viable material used in a medical device, but later the reference to non-viability was removed. In 1999, the preferred definition proposed, that a biomaterial was a material intended to interface with body and the scope of biomaterials was solely within the domain of health care. Also other opinions were presented: a biomaterial was defined as a solid material which occurs in and is made by living organism. In 2009, Williams concluded that a biomaterial is a substance that has been engineered to take a form which is used to direct the course of any therapeutic or diagnostic procedure in medicine. The definition states that a biomaterial can be for example metallic or ceramic and it does not have to be of biological origin as long as it interacts in body in desired manner. [14]

3.1 History of orthopedic biomaterials

Only 60 years ago the concept of biomaterials was not used. There were no implantable devices, formalized regulatory approval processes and understanding of biocompatibility. However, crude biomaterials have been used throughout human history generally with poor or mixed results. [15] According to archaeological evidence orthopedic procedures were performed in several ancient civilizations, yet frequently surgical methods leaded to amputation rather than repair. [1]

Prior to 1950 most implants had a low level of success because of a poor understanding about biocompatibility and sterilization. [15] Nor was the knowledge of the musculoskeletal system fully understood. Early hip arthroplasties provided groundwork for the current field of orthopedics, fixation methods, and medical devices. The evolution of total hip replacement includes advancements in processing of materials and improved understanding of physiological conditions. [1]

The first hip replacement was performed in 1891 using a cemented ivory ball. The implant was not successful. Between 1920 and 1950, numerous attempts were made to develop hip and knee prostheses. Materials like glass, acrylic, Teflon, chrome-based alloys, stainless steel, and other metals and alloys were used. The implants have been failed due to poor durability and harmful wear products. The first

successful hip joint prosthesis was implanted 1961 and consisted of a ultra-high-molecular-weight polyethylene (UHMWPE) cup with femoral stem and a ball head made of cobalt alloy. [15] Compared with older materials, UHMWPE provided resistance to corrosion, fatigue and wear. UHMWPE and cobalt alloys are still used in total hip arthroplasty and they have undergone extensive improvements in processing, structural development, and manufacturing over 50 years. The fixation between the proximal end of femoral stem and bone is now achieved with press fit methods, acrylic bone cement, or porous coatings. Stability of an implant can be improved by cables, screws and rods. More recent developments are porous titanium or cobalt-chromium coatings on the femoral stem to enhance bone integration and introduction of crosslinked forms of UHMWPE for improved wear resistance. [1]

In 1952 it was observed that titanium integrates into the bone tightly. The phenomenon was named osseointegration. Nowadays titanium and its alloys are used in most dental implants and in many other orthopedic implants. [15]

3.2 Requirements for orthopedic biomaterials and scaffolds

In the first generation of implantable devices, between the years 1940 and 1980, the best performance was achieved with materials that were the least chemically reactive. Implantable materials were selected and developed in such way that failure could be avoided. Materials in these long-term implantable devices had to be e.g. non-toxic, non-immunogenic, non-thrombogenic, non-carcinogenic and non-irritant, in other words the materials had to be biologically safe. These requirements defined the concept of biocompatibility. Biocompatibility was also defined as the implant's ability to exist in contact with the tissues of human body without causing an unacceptable degree of harm to the body. [16]

Nowadays there are also implantable devices which are not intended to remain within an individual for a long time. Some applications require that the material reacts with tissues or degrades over time rather than stays inert. The application site affects as well: the response to a material can vary depending on site. Therefore biocompatibility was redefined in 1987 by David F. Williams as follows: "*Biocompatibility refers to the ability of a material to perform with an appropriate host response in a specific situation.*" [16]

Biocompatible materials can be divided into different categories: bioinert, resorbable and bioactive materials. [5] Thin connective tissue capsules are formed around bioinert (biotolerant) materials. The capsule does not adhere on the implant surface. Bioresorbable materials resorb in the body and autologous tissue replaces the material. Bioactivity is usually interconnected with bone tissue. Bone tissue is formed around the bioactive implant, which strongly integrates with surrounding tissue. [2]

Accordingly, biocompatibility is the most important aspect with implantable devices. There are also other important factors that affect the success of the implant. These factors are for example related to the mechanical properties of material and the performance of material in the implant site. In respect to scaffold, the porosity and pore size, as well as the scaffold's surface properties have to be considered.

The bone scaffold should serve as a template for cell interactions and for the formation of a bone extracellular matrix. The scaffold should also provide a structural support for new bone tissue. If the scaffold is biodegradable, the rate of biodegradation should meet the rate of bone remodeling. [6]

Biological environment is harsh for implantable devices. Implants are constantly in contact with extracellular tissue fluid with a salt content of about 0.9 % at pH 7.4 and temperature of 37±1°C. The electrolytes in body fluid are sodium, chloride, and bicarbonate, and small amounts of potassium, calcium, magnesium, phosphate, and sulphate. There are also amino acids, proteins, plasma, lymph etc. [13] Implantable devices have to stand up in such an environment.

An ideal bone replacement scaffold is osteoconductive, osteoinductive, and osteogenic. Osteoconductive means that the scaffold favors ingrowth of a new bone tissue. [17] Osteoconductive materials bind to bone and stimulate bone growth along the surface of the material. [5] The osteoconductive material provides a surface for cells to attach, proliferate, and deposit bone matrix [18]. Osteoconduction is the primary purpose of the scaffold material [6]. In osteoconduction, the biomaterial acts as a scaffold for new bone that grows from neighboring living bone. A scaffold is osteoinductive when it induces the transformation of osteoprecursor cells from the host into bone matrix producing cells [18,19]. The scaffold can contain cytokines, such as bone morphogenetic proteins, that cause the osseoinduction. Osteogenesis occurs when the scaffold is seeded before implantation with cells that

will establish the new centers of bone formation. [6] Osteogenic material has the intrinsic capacity to stimulate bone healing [18].

The concept osseo- or osteointregration is described as a direct bone-to-biomaterial interface without fibrous tissue. Osseointegration is useful, because greater forces can be transferred along integrated bone interfaces. It also eliminates or minimizes interfacial movement or a slip. [15] Without osseointegration, fibrous tissue is formed between the bone and the implant. Therefore, an appropriate surface material is extremely important for implant success. The surface chemistry, surface roughness and surface topography are important issues regarding osseointergation. [2]

The orthopedic scaffold should have proper mechanical properties to allow load-bearing. [17] Mechanical properties should be similar to those of bone repair site [6]. Stress shielding occurs when a scaffold is much stronger than bone [8,20,21]. A high rigidity implant can induce bone atrophy due to the absence of mechanical stress. Lower rigidity may delay or minimize the bone atrophy due to the mechanical stress. [22]. This bone resorption around the implant can consequently lead to implant loosening. The resorption is due to the stress shielding effect that leads to death of the bone cells. The implant's fracture due to inadequate strength or the mismatch in mechanical properties between the bone and implant is called biomechanical incompatibility. [2]

3.2.1 Porosity

Porosity and pore size are important factors in bone formation *in vitro* and *in vivo*. Porosity is defined as the percentage of empty space in solid. The pores are necessary for the bone tissue ingrowth and formation because they allow the migration and proliferation of osteoblasts and mesenchymal cells. The pores are also important for vascularization. [6] The pores have to be open and interconnected to allow the above-mentioned functions. [5,23,24] The apertures between the pores should have diameters over 100 µm. [5] The interconnectivity is also essential for the diffusion of nutrients. [23]

Higher porosity enhances osteogenesis. Thus, highly porous implants are preferred for bone regeneration. Even though the increase in pore size and porosity enhances

the bone ingrowth, it results in decreased mechanical properties. This is a critical aspect in load-bearing implants. [6]

Kuboki *et al.* [25] showed the importance of porosity in bone regeneration. They compared solid particles of HA with porous ones. Particles were mixed with bone morphogenetic protein 2 (BMP-2). Porosity was 70 % and a pore size 150 µm. Direct osteoneogenesis occurred only in the porous scaffolds and no new bone was formed on the solid particles. [25]

Porosity can be classified on the basis of the pore size. Macroporosity has a pore size greater than 50 µm and microporosity less than 10 µ. [6] In the literature, there are several results for optimal pore size [5] but no consensus [24,26]. Most studies suggest that the optimal pore size for bone ingrowth is 200-600 µm [27]. The minimum pore size required to generate mineralized bone is generally considered to be about 100 µm. The minimum pore size for angiogenesis, the formation of new blood vessels, is also 100 µm [5]. Unmineralized bone tissue grows into smaller pores 75-100 µm, whereas only fibrous tissue penetrates into even smaller pores (< 75 µm). However, scaffolds with smaller pore sizes have also shown bone ingrowth under non-load-bearing conditions. Studies have shown better osteogenesis for implants with larger (> 300 µm) pores, because they allow vascularization and high oxygenation although the type of bone ingrowth depends on the biomaterial and the geometry of pores. [6]. The optimal pore sizes can be compared with normal haversian systems that reach an approximate diameter of 100-200 µm [6].

Even though macroporosity is important to new bone formation, also microporosity and the surface topology are significant. The nanometer scaled surface roughness and nanometer-sized pores on the surface can increase the cell activity. [5] A porous surface improves the mechanical interlocking between the implant and the bone. The surface roughness also enhances the attachment, proliferation and differentiation of anchorage-dependent bone forming cells. [6]

The internal architectural design of scaffolds may have a control over the overall geometry of newly formed bone. Cylindrical HA implants with two architecture designs, orthogonal and radial channels, were studied *in vivo*. Although the percent of the bone ingrowth was not statistically different, the overall shape of the regenerated bone tissue was significantly different. The orthogonal architecture resulted in an interpenetrating matrix, whereas in the radial design the regenerated

bone formed an intact piece at the center of the implant. [28] Also the pore geometry may affect bone formation. Longer and curved pores have been observed to hinder the penetration of mesenchymal cells and capillaries, which resulted in bone formation only on the outer surface of the hydroxyapatite implant. On the contrary, particle system scaffolds resulted in bone regeneration deeper in the material. [6]

3.2.2 Biocompatibility

Bone grafts are used to replace faulty or damaged parts of the body [29] for example in replacement of bone after removal of a tumor, in revision surgery of failed hip prostheses and in fusion of vertebrae. The bone grafts are divided to autografts and allografts. The autograft is patient's own bone and its use is preferred. However, this is not always possible due to an insufficient supply of bone available or a poor quality of bone. [5] The allograft is taken from one individual and implanted in another of the same species. The process is called transplantation. [29] In addition to autografts and allografts, synthetic materials are used to replace bone, especially when autografts and allografts are not available. To improve biocompatibility of the synthetic implant, bioactive materials can be used.

By definition, a bioactive material is one that elicits a specific biological response at the interface of the material, which results in the formation of a bond between the tissue and the material. There are two classes of bioactive materials: osteoconductive and osteoproductive (also called osteoinductive). Osteoconductive materials conduct bone growth along the surface of material and osteoproductive materials stimulate the growth of new bone on the material away from the bone/implant interface. [5]

Synthetic hydroxyapatite (HA) and tricalcium phosphate (β-TCP) ceramics are both calcium phosphate ceramics and similar to the bone mineral. They are osteoconductive, crystalline materials, whereas bioactive glasses are osteoproductive and amorphous. Tri-calcium phosphate and certain bioactive glasses are resorbable. HA resorbs also, but very slowly. The dissolution products of HA do not stimulate the genes in the osteogenic cells. Therefore HA is only osteoconductive and can act as a bone replacement material rather than a regenerative material [5]

HA ($Ca_{10}(PO_4)_6(OH)_2$) forms when β-TCP ($Ca_3(PO_4)_2$) combines with calcium hydroxide ($Ca(OH)_2$) [3]. The rate of dissolution depends on the calcium-phosphorus ratio. Compounds with Ca:P ratio lower than 1:1 are not suitable for biological implantation. This is because their solubility and speed of hydrolysis increase with the decreasing hydrolysis Ca:P ratio. Therefore, β-TCP with Ca:P ratio 1.5 is more rapidly resorbed that HA with Ca:P ratio 1.67. [15]

Many bioactive silica glasses are based upon the formula called 45S5, which contains 45 w% SiO_2 and 5:1 ratio of CaO to P_2O_5. Glasses with lower ratios do not bind to the bone. [15] 45S5 is also the first and well-studied composition of Bioglass™. The base components in most bioactive glasses are SiO_2, Na_2O, CaO, and P_2O_5. [30] Compositions of different bioactive glasses under the trademark Bioglass™ are presented in Table 3.

Table 3. Composition (w%) of different Bioglass™ formulas. [30]

Component	45S5 Bioglass™	45S5.4F Bioglass™	52S4.6 Bioglass™	55S4.3 Bioglass™
SiO_2	45	45	52	55
P_2O_5	6	6	6	6
CaO	24,5	14,7	21	19,5
Na_2O	24,5	24,5	21	19,5
CaF_2		9,8		

After the immersion in body fluid, a hydroxycarbonate apatite layer is formed on the bioactive glass surface. The apatite layer is similar to the apatite layer in bone. This is assumed to be the basis of the reactivity of the glass [5]. The bone can chemically bind to the formed bioactive layer [31]. Bioactive glasses form a bond to the bone much quicker than ceramics. Moreover, bioactive glasses can bond to soft tissue. [5]

Usually, ceramics have a high compressive strength and Young's modulus and a low toughness and therefore they are brittle materials. The composition, structure and Young's modulus of HA resemble those of bone. Porous HA and β-TCP can be both colonized by bone tissue. [5]

3.3 Biodegradable polymers in orthopedics

Biodegradable polymers can be divided into two major classes: natural and synthetic. The division is made by the origin of polymer, not by the structure. Therefore the polymers in these classes have properties that vary widely inside the class. In general, synthetic polymers can have more application areas because they can be tailored to give wider range of properties. On the other hand, some natural polymers have functional groups suitable for tissue engineering and they are less prone to produce toxic effects. However, the functional groups and possible contaminants present in natural polymer can also produce unwanted immunological effects. [32]

The properties of biodegradable polymers can be customized by using copolymers. In biomedical applications, requirements include suitable mechanical strength, degradation time, surface properties and physicochemical parameters. In addition, the presence of functional groups effect on the properties of polymer in body. In bone repair the mechanical properties are particularly important. [32]

By definition, biodegradation is the chemical breakdown of materials by the action of living organisms. It leads to changes in their physical properties. [15] A biodegradable polymer is not always bioresorbable. Bioresorbable polymers are eliminated totally in the body with no residual side effects. [33] Therefore, a biodegradable polymer used in a medical device should be bioresorbable and it should degrade and/or be removed completely in body. The degradation should take place in a predictable manner and the degradation products should not cause any undesirable effects at the implantation site or on any other body organs or functions. [32]

The polymer matrix degrades by a hydrolytic and/or enzymatic attack. The degradation processes can be divided into bulk and surface erosion. In a bulk erosion process a polymer loses mass uniformly throughout the matrix and the degradation rate depends on the volume of the polymer rather than its thickness. [32] The molecular weight reduces in the entire polymer matrix and monomers or oligomers diffuse out. [33]

In a surface eroding process degradation starts from the surface and continuously moves to the core of the polymer matrix. The lifetime of the polymer device is dependent on the thickness and therefore the thicker the device is, the longer the

lifetime is. [32] Polymer backbone is cleaved only on the surface and monomers and oligomers diffuse into the surroundings. Therefore the molecular weight inside the polymer does not usually change. [33]

4 Titanium scaffolds

The most commonly used metals in orthopedics are stainless steel, cobalt-chrome (Co-Cr) alloys and titanium (Ti) alloys. The preferred titanium alloy used for implants is $TiAl_6V_4$. Aluminum and vanadium stabilize the titanium phase and result in excellent mechanical strength. The elastic modulus of $TiAl_6V_4$ is lower compared with stainless steel and Co-Cr alloys, which can decrease the stress shielding of bone. [5] Titanium and its alloys exhibit the most suitable characteristics for biomedical applications due to their high biocompatibility, specific strength, and corrosion resistance [11].

Titanium has been used in several orthopedic applications. These include hip stems, joints, and osteosynthesis material such as screws, plates and nails [34]. Titanium has been most commonly used material for over 40 years for fabrication implants for dental and orthopedic purposes. [26] It seems that titanium alloys are now going to be the first choice of material for majority of orthopedic applications. [2]

4.1 Properties of titanium and its alloys

Ti and its alloys have an excellent corrosion resistance in physiological medium [23]. This is due to the formation of a very stable TiO_2 oxide phase on the metal surface [5]. The oxide layer forms spontaneously and the thickness of the layer is up to 7 nm [35]. Ti and its alloys are mainly used in implants that replace hard tissue, such as artificial hip joints and dental roots [11].

Commercially pure (CP) titanium and its alloys have good mechanical properties. They have a high strength-weight ratio, low elasticity modulus and fatigue strength compared with other metals. [23] CP titanium and $TiAl_6V_4$ ELI (Ti64, Extra Low interstitial) are the most commonly used titanium materials for implant applications [2]. The ultimate tensile strength of Ti64 is 900 MPa and the modulus of elasticity is 110 GPa. [5] Ti64 is claimed to have a strength about 100 % higher compared to pure titanium. Al and V ions might have some toxic effects. However, these might not be released during long-term use and only minor ion release has been reported from clinically used implants. [36]

The Young's modulus for bulk titanium alloy is 40 GPa at its lowest. That is greater than Young's modulus of cortical bone, which is approximately 10-30 GPa. The mechanical properties of titanium and the mechanical biocompatibility of an implant can be changed with increasing porosity. An effective way to reduce the Young's moduli of titanium and its alloys is to increase the porosity. [11]

4.2 Preparation of porous titanium

There are several different ways to manufacture porous titanium. The preparation method has effects on porosity, pore size, the interconnectivity of pores, and the mechanical behavior of the scaffold. Available manufacturing techniques are e.g. electron beam melting (EBM), laser additive manufacturing processes, powder manufacturing process, environmental-electro-discharge-sintering [37], freeze casting, and rapid prototyping [24]. Random pores are formed in freeze casting [24] and powder manufacturing processes [9], whereas laser additive manufacturing [34], rapid prototyping [38] and electron beam melting [12] form a controlled architecture.

4.2.1 Powder manufacturing process (with sintering)

Porous scaffolds can be manufactured using titanium powder. Oh *et al.* fabricated porous titanium scaffolds by controlling sintering conditions and powder sizes. The powders were sintered in a vacuum at different temperatures. The resulting scaffolds were porous and the pores were interconnected. Figure 6 illustrates the surface of manufactured scaffolds. [9]

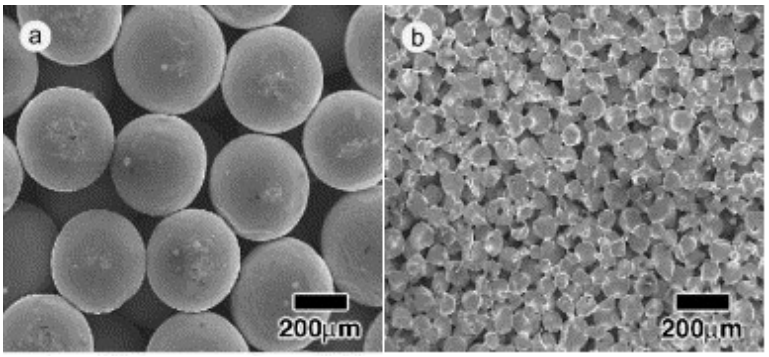

Figure 6. SEM micrographs of porous Ti compacts sintered at (a) 1300 °C with 374 μm powder and (b) 1100 °C with 65 μm powder. [9]

The space-holder technique is a powder manufacturing process. It allows the manufacturing of titanium foams with designed porosity. The choice of space-holder effects on the porosity, the pore size and pore morphology [39]. The space-holder is removed after sintering. Most space-holders are completely evaporated at low temperatures or are removed by a dissolution process. However, the toxicity of the space-holder is of a great concern, because it is difficult to ensure that it is completely removed from the foam. [37] Typical space-holders are for example sodium chloride (NaCl) [37], ammonium hydrogen carbonate and carbamide [39].

Müller *et al.* prepared porous titanium scaffolds by powder metallurgy according to the space-holder procedure. They used commercially pure (CP) titanium powder. After sintering step (1200 °C) the scaffolds were treated with ethanol and ultrasonic to get rid of possible air pockets. The porosity was 65-70 % and pore size was 100 – 700 μm. The majority of pores were between 250 and 500 μm (Figure 7). [35]

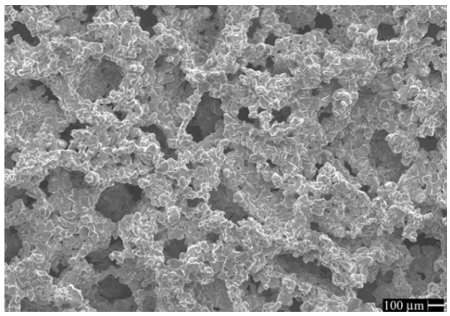

Figure 7. SEM micrograph if CP titanium foam, with porosity of 65-70 % and pores with a diameter of 350 to 550 μm. [35]

4.2.2 Titanium foam

Titanium foams can be made different ways. Titanium foam can be produced by mixing titanium powder with organic solid binder powder and a foaming agent. The powder mixture is heated and the organic binder melts and foam forms. The result is a solid foamed structure comprising titanium particles and the organic binder. The structure is heated to eliminate the organic binder and finally sintered the remaining three-dimensional network with interconnected porosity. [40] This type of titanium foams have been successfully tested as implants in the rabbit femurs and the tibias of rats. [41]

Another way to manufacture titanium foam has been used. Titanium foam is made by impregnating a form made of open-cell polyurethane (PU) foam with solution consisting of titanium powder and binding medium. PU and binding agents are vaporized and the remaining titanium is sintered (Figure 8). [42]

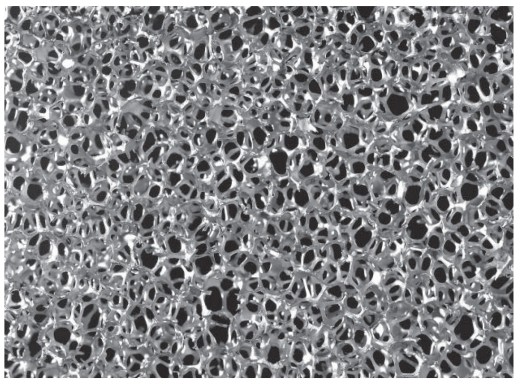

Figure 8. Titanium foam. [42]

4.2.3 Laser additive manufacturing

Laser additive manufacturing (AM) includes laser sintering (LS), laser melting (LM) and laser metal deposition (LMD). Different phrases are used depending on the institutions and companies. AM consolidates and shapes the feedstock (typically powder material) layer by layer and normally uses a computer controlled laser as the energy source. [34]

LS is based on spreading powder layer by layer and subsequent laser sintering. LS system normally consists of a laser, an automatic powder layering apparatus, a computer system for process control and some accessorial mechanisms. Different types of lasers are used and they influence on the consolidation of powder because of the different wavelengths and energy densities of lasers. In LS process, the laser melts the powder only partially. Therefore powder characteristics and laser processing conditions have to be carefully determined. [34]

LM has the same processing apparatus and procedures as LS. The only difference is that metallic powder melts completely in LM. In recent years, laser processing conditions have continuously improved. This leads to improved microstructural and mechanical properties. LM processed material shows a better densification rate, surface smoothness and microstructural homogeneity under optimal processing conditions compared with LS processed material. Nonferrous pure materials can be processed with LM, but LS process is not suitable for pure metals. However, LM requires high laser power, higher energy level, thin powder layers and longer building time. [34]

In LS and LM the powder supply is pre spread, whereas in LMD powder is fed coaxially. In LMD the powder is fed in a gas delivery system. The laser beam and powder are focused on the same place and moved in the z direction to control the height of the scaffold. The workpiece is moved in the x-y direction by the computer controlled drive system under the beam/powder interaction zone, which forms the cross-sectional geometry. The geometry formed can be complex and have high dimensional accuracy. [34]

4.2.4 Rapid prototyping

Rapid prototyping (RP) combines computer-aided design (CAD) with computer-aided manufacturing (CAM) and builds objects with predefined microstructure and macrostructure. Traditionally, RP has concentrated on polymeric and ceramic materials. RP can also be used to manufacture porous Ti scaffolds. [38]

Li *et al.* used $TiAl_6V_4$ powder to prepare porous scaffolds. First, $TiAl_6V_4$ powder was mixed with an aqueous solution of methylcellulose and stearic acid to obtain slurry. Second, the scaffold was formed by RP and the samples were dried. Finally,

scaffolds were sintered in a high vacuum furnace. A fully interconnected porous network with highly controllable porosity and pore sizes was formed (Figure 9). [38]

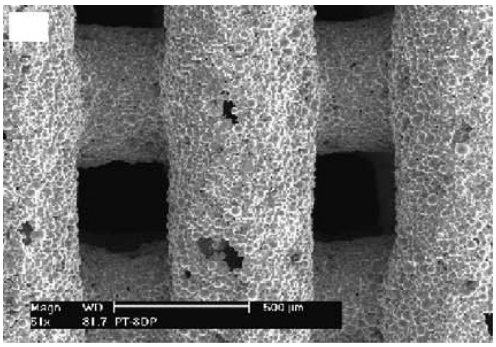

Figure 9. Environmental scanning electron microscope (ESEM) micrograph of $TiAl_6V_4$ scaffold. Optimal concentration (66 vol% $TiAl_6V_4$ powder used). [38]

4.2.5 Electron beam melting

Electron beam melting (EBM) can also be considered as one branch of AM. The first step in EBM is to create a three-dimensional model with CAD. The geometrical data of the component is sliced into layers with constant thickness, because the component is generated layer by layer. A fully interconnected porous network and highly controllable porosity and pore size can be manufactured with EBM. [43] The thickness of one layer is 100 µm [44], [45]. Components can be built up to size of 150 mm x 150 mm x 180 mm [45]. The production of EBM components is performed under a vacuum atmosphere (10^{-4}-10^{-5} mbar). This is especially important for titanium due to its high affinity to atmospheric gases like oxygen and nitrogen. [12]

EBM machine reads the data from a CAD model and melts the first 100 µm metallic powder layer. [44] The process platform is lowered by the thickness of one layer and the process is repeated until the component is built. The process takes place in a powder bed. The metal powder which is not molten during the process supports the forming component. [12] The schematic picture of EBM process is presented in Figure 10.

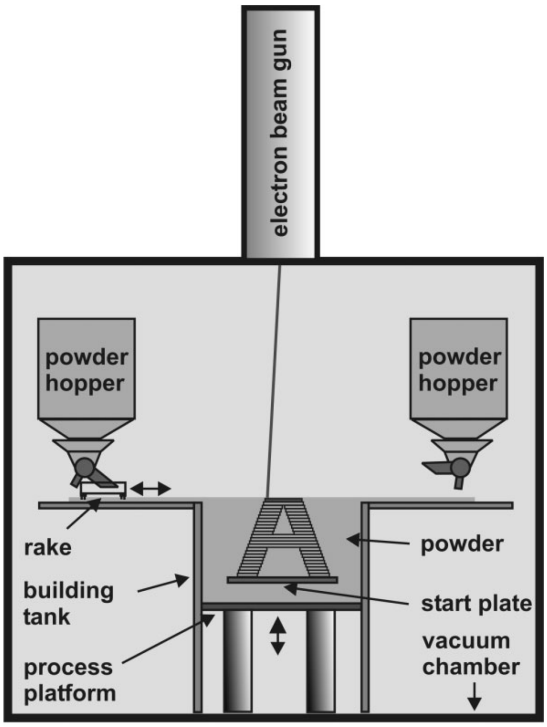

Figure 10. Schematic picture of Arcam EBM system [43].

The component is cooled down either under a vacuum or helium atmosphere. The supporting powder is removed by powder blasting with the same powder as used in the building process. Therefore, the remaining powder can be reused after sieving in a new process. [12] Figure 11 shows a network manufactured by FIT Fruth Innovative Technologies Ltd and used in the experimental part of this thesis.

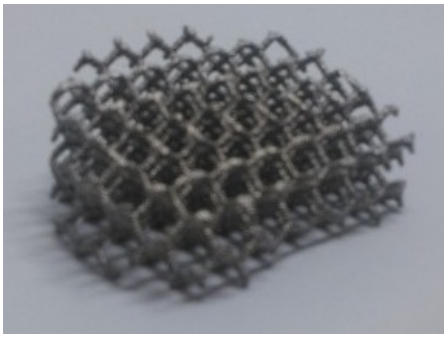

Figure 11. Picture of cylindrical network manufactured by FIT Fruth Innovative Technologies Ltd.

Heinl et al [12] studied EBM manufactured titanium alloy ($TiAl_6V_4$, Ti64) networks with different process settings and pore sizes (Figure 12). They concluded that the mechanical properties of porous EBM manufactured titanium alloy depend on the relative density, pore architecture (open or closed pores) and anisotropy. Increasing the relative density raises the elastic modulus. The lowest relative density was achieved with the highest porosity of 87 %, largest pore size (strut length) of 1.8 mm and strut thickness of 0.4 mm. The process settings affect on the thickness of the struts in the network. For the material with the lowest density (0.13 g/cm^3), the compressive strength at break was 16.3 MPa and elastic modulus 0.4 GPa. The porosities of structures were between 60 % and 87 % and the relative densities were between 0.13-0.40 g/cm^3. Pore diameters varied between 0.67 and 1.82 mm. With the highest relative density the compressive strength at break was 118.8 MPa and elastic modulus 6.5 GPa. [12] Therefore, the mechanical properties can be adjusted by altering the process settings and pore sizes in EBM manufactured networks.

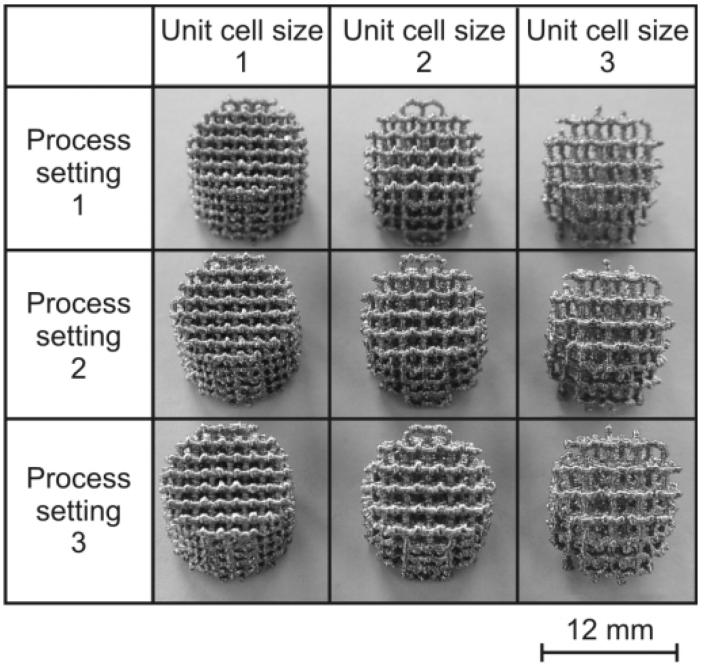

Figure 12. EBM manufactured titanium alloy networks. [12]

Cheng *et al.* [21] studied the compression deformation behavior of EMB manufactured Ti64 meshes with different porosities and strut sizes. With 86 % porosity, 3 mm strut length, 1 mm strut thickness and 0.62 g/cm^3 relative density, the compression stress at break was 12.4 MPa and the compressive modulus was

0.54 GPa. As the relative density was increased to 0.73 g/cm^3, the compression stress at break was 20.9 MPa and the compressive modulus was 0.89 GPa. However, they received also higher value for compression stress at break (113 MPa) when the relative density was even higher (1.68 g/cm^3) [21]

Hrabe *et al.* [20] performed fatigue testing for EBM manufactured titanium alloy ($TiAl_6V_4$) networks. They observed a reduced fatigue lifetime compared to the expected value and proposed three possible reasons for that. First, µCT images revealed closed porosity within the struts, which may yield stress concentrations. Second, sintered particles and texture lines on the surfaces of struts may also yield stress concentrations. Third, the microstructure of EBM manufactured $TiAl_6V_4$ (acicular α or martensite) is not optimal for high-cycle fatigue resistance. [20]

Ponander *et al.* [46] cultured human osteoblasts *in vitro* on the surface of EBM manufactured $TiAl_6V_4$ scaffolds. The scaffolds had different surface roughness. After few days of incubation, osteogenic proliferation and differentiation genes were expressed. The cells were able to attach, proliferate and differentiate on $TiAl_6V_4$ specimens with different surface types. [46]

Palmquist *et al.* studied EBM manufactured $TiAl_6V_4$ meshes. They performed experimental studies in sheep. The study demonstrated osseointegration and high bone-implant contact throughout the porous scaffold. The porous implants showed also good long-term soft tissue biocompatibility and expressed thinner fibrous encapsulation compared to solid implants. [36]

Applications for EBM manufactured Ti64 meshes has already been proposed. Li *et al.* designed acetabular cup with porous structure, cranial implant (Figure 13) and local porous structure for joint prosthesis. [47] Murr *et al.* proposed also acetabular cup design. Other fabricated orthopedic implant prototypes were a total knee implant and a tibial (knee) stem (Figure 14). [48] Li *et al.* proposed an EBM manufactured implant to repair a mandibular bone defect [27].

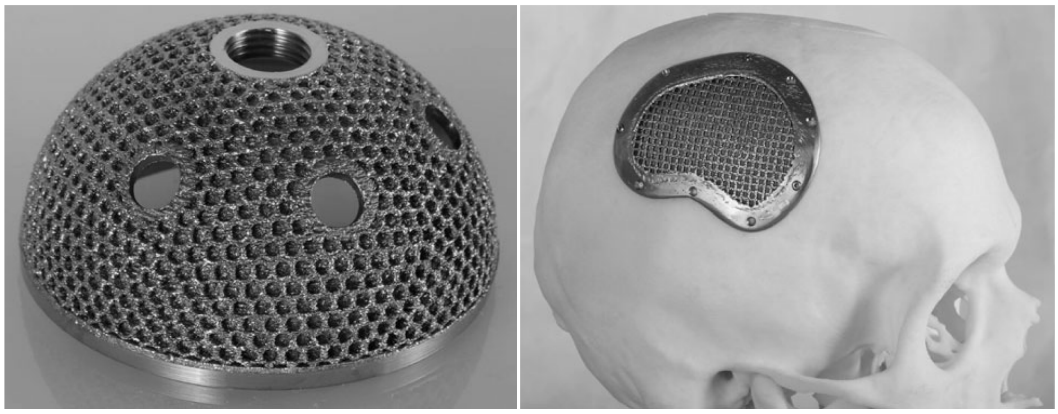

Figure 13. EBM manufactured acetabular cup and cranial implant [47], modified.

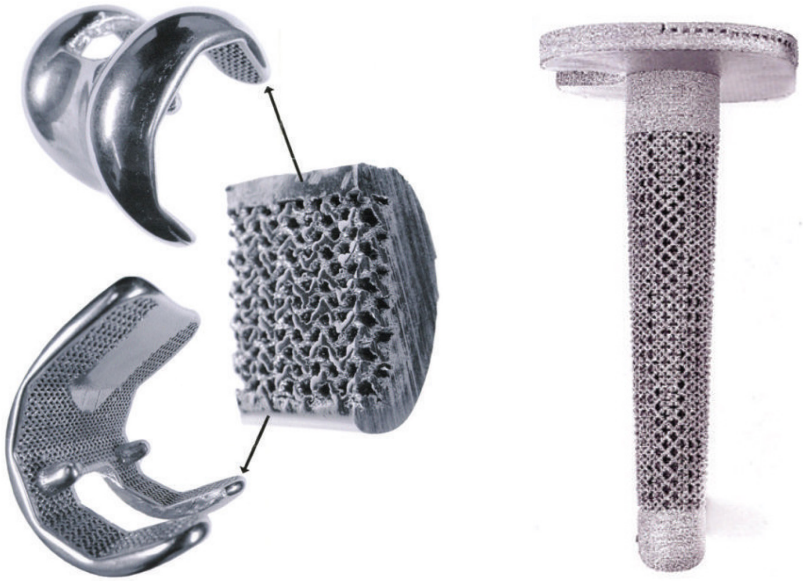

Figure 14. Total knee implant and tibial stem [48].

FDA has approved a product from Limacorporate S.p.a., which includes EBM manufactured Ti64. The Delta TT Acetabular System is a hip joint prosthesis. The Delta TT cup is manufactured using an EBM (Figure 15). [49]

Figure 15. The Delta TT cup [50]

5 Porous titanium/polymer hybrid materials

There are different objectives to manufacture titanium/polymer hybrid materials, such as improving biocompatibility and mechanical properties. The application area for titanium/polymer hybrid materials is in orthopedics.

Porous titanium has a good biocompatibility. However, it can be improved by filling the titanium pores with a polymer that exhibits biofunctionalities. [51] The elastic modulus of solid titanium is much higher than the one of cortical bone. The elastic modulus can be lowered by manufacturing porous materials. On the other hand, increasing porosity impairs also the mechanical strength of a titanium scaffold. The mechanical strength decreases due to the structural defects and the stress concentration around the pores. Therefore, a polymer filling can also be used to improve the mechanical properties. [52]

Porous titanium used in titanium/polymer hybrid materials can be manufactured in different ways. The most common is the powder manufacturing process which is presented in the following review of literature. Used polymers are non-biodegradable high-density-polyethylene (HDPE), polyurethane (PU) [52] and polymethylmetacrylate (PMMA) [53], and biodegradable poly-L-lactide (PLLA) [51,54,55]. The polymer matrix can be non-porous or porous depending on the desired properties.

5.1 Hybrid materials with non-biodegradable polymer

The objective for manufacturing porous titanium/non-biodegradable polymer hybrid materials is to produce a material with mechanical properties comparable to those of human bone. Nakai *et al.* [10] manufactured titanium scaffolds with different pore sizes and porosities. The pore sizes and porosities depended on titanium powder particle sizes, sintering temperatures, and manufacturing pressures. Titanium scaffolds were filled with PMMA. The PMMA filling increased the tensile strength of porous titanium with highly porous scaffolds. The effect of the PMMA filling on the Young's modulus was not remarkable because the Young's modulus of PMMA is considerably lower than that of porous titanium. PMMA filling may affect negatively on osteoconductivity of titanium. Figure 16 shows SEM picture of porous titanium and porous titanium/PMMA hybrid material with 45 % porosity. [10]

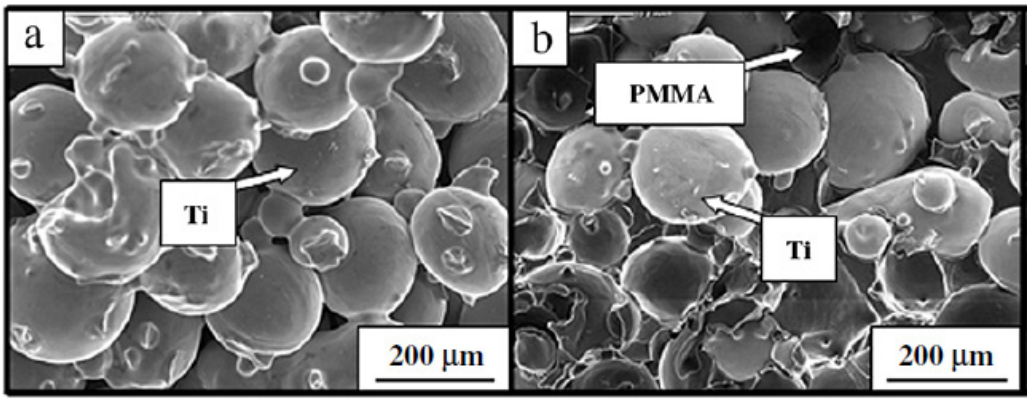

Figure 16. SEM micrographs. A. Porous titanium. B. Porous titanium/PMMA hybrid material. [10]

Wang *et al.* [52] used HDPE and PU to fabricate porous titanium/polymer hybrid materials. The porosity and pore sizes were controlled by varying the sintering process parameters. The pores were open and interconnected when porosity was over 25 %. The polymers were impregnated into the scaffold with the assistance of hydraulic pressure. Normal impregnating processes are capable of filling mainly over 125 µm pores. However, with hydraulic assisted system high viscosity polymers, such as HDPE and PU, can be impregnated into porous titanium with a pore size as small as 10 µm. Figure 17 shows titanium powder, porous titanium and titanium/polymer hybrid materials used in the study. [52]

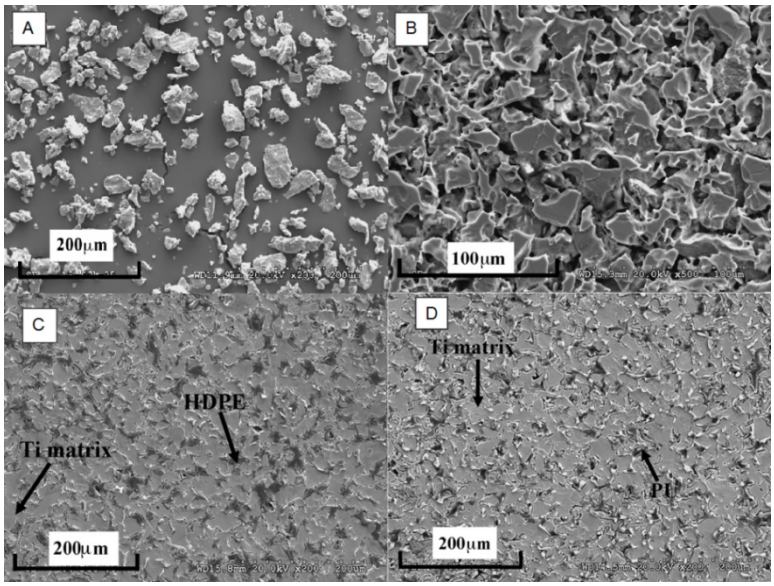

Figure 17. SEM micrographs. A. Titanium powder. B. Porous titanium, porosity 35 %. C. Titanium porosity 37 %, Titanium/HDPE porosity 0%. D. Titanium porosity 37 %, Titanium/PU porosity 0%. [52]

5.2 Hybrid materials with biodegradable polymers

Nakai *et al.* [51] studied hybrid materials further and replaced PMMA with PLLA. Porous titanium was fabricated through the powder manufacturing process. L-lactide was polymerized to PLLA inside the porous titanium in a nitrogen atmosphere under a vacuum at 160 ºC for 1h. PLLA did not have a remarkable effect on Young's modulus or tensile strength. However, PLLA increased the compressive strength with highly porous titanium scaffolds. Figure 18 shows SEM micrographs of titanium with 45 % porosity filled with PLLA. [51]

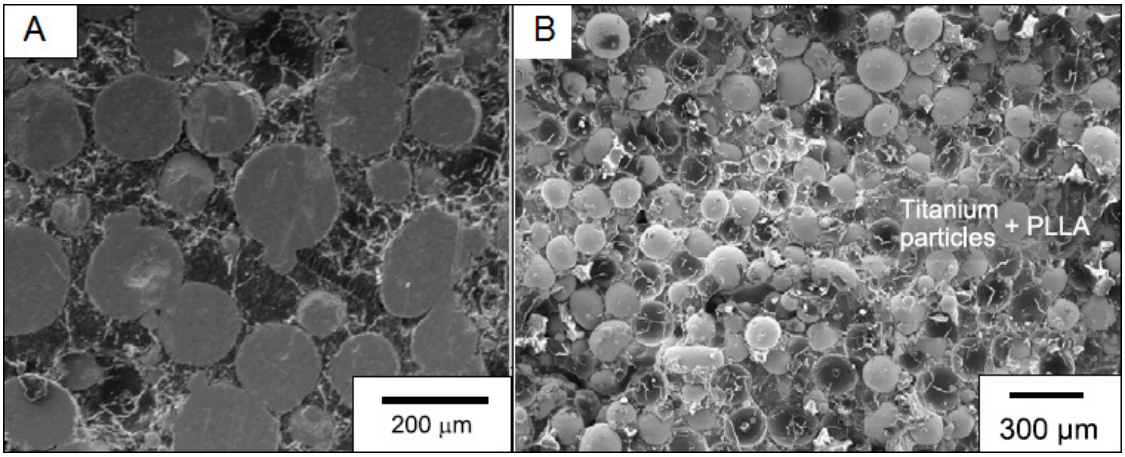

Figure 18. SEM micrographs. A. surface of porous titanium filled with PLLA. B Cross-section of porous titanium filled with PLLA. [51]

PLLA filling in the pores degrades during immersion in Hank's balanced salt solution (HBSS). HBSS is a stimulated body fluid which includes organic components (Na^+, K^+, CA^{2+}, Mg^{2+}, HCO_3^-, Cl^-, HPO_4^{2-} , and SO_4^{2-}) [56], but no cells or biological polymers. The energy dispersive X-ray spectroscopy (EDX) results indicate calcium phosphate formation after eight weeks immersion. After twelve weeks immersion X-ray diffraction (XDR) profile proved the formation on hydroxyapatite. [51]

The PLLA degradation rate increases with a prolonged immersion time. However, after eight weeks immersion the weight loss rate of the material becomes low. This may have two reasons: formation of HA on the surface of material increases weight and/or decreases the degradation rate of PLLA. The decrease of the degradation

rate is due to smaller the contact area with HBSS by covering of the surface of the material. [51]

Watanabe *et al.* [54] also used porous titanium and PLLA to fabricate hybrid materials. Porous titanium was fabricated through mixing titanium powder and NaCl and sintering the titanium matrix. Porous titanium was obtained by dissolving the NaCl in water. PLLA was melted and introduced into the pores of titanium samples under vacuum. PLLA did not fill the pores thoroughly and the amount of bubbles varied from place to place. PLLA reinforced the titanium matrix but there was a mechanical gradient. Figure 19 shows porous titanium with 50 % porosity filled with PLLA. [54]

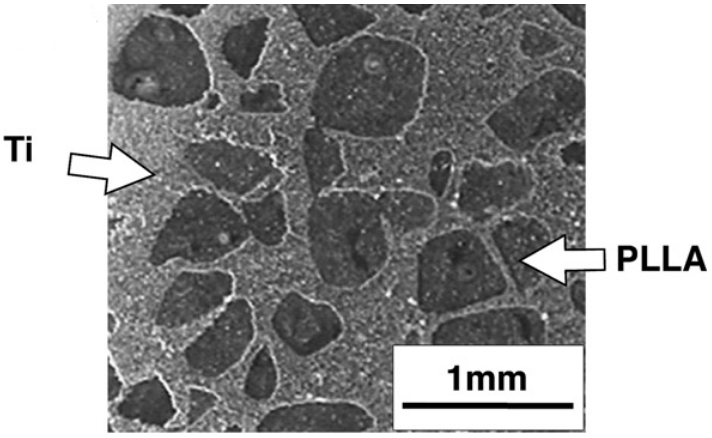

Figure 19. Optical microscope image of titanium/PLLA hybrid material. [54]

5.3 Hybrid materials with porous biodegradable polymer

Hybrid materials with a porous polymer matrix are not studied extensively. Vrana *et al.* [55] used porous titanium manufactured by fusing spherical titanium microbeads (Figure 20A). In other words, they used the powder manufacturing process. The biodegradable polymer used was PLLA. Porous polymer was manufactured using the freeze extraction method, which is easy to scale up. Freeze extraction is a thermally induced phase separation technique. The method forms open, interconnected pores via extraction of the frozen solvent from frozen polymer solution via a non-solvent for the polymer. The solvent can be for example dioxane

and non-solvent ethanol. The pores were formed with a Teflon mold that directs the process and permits a formation of pore gradients. The mold directs the movement of the extraction fluid. The morphology of polymer pores was similar with and without titanium and the titanium scaffold was totally engulfed by the polymer network (Figure 20B). [55]

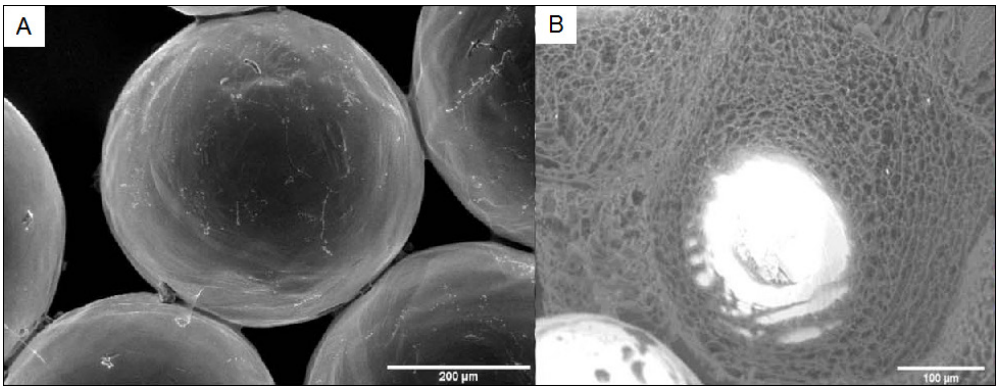

Figure 20. A. SEM image of porous titanium. B. ESEM image of porous titanium/porous PLLA hybrid material. [55]

6 Spinal implants

Scoliosis and related back pain, loss of motion, and spinal fracture are reasons for the need of spinal implants. Disc arthrosis and collapse also require medical treatment. One of the most common causes of back pain is degenerative disc disease (DDD) of the intervertebral discs which results in a loss of disc height and mechanical function. [1] Conservative treatments for back pain are bed rest, anti-inflammatory medications, and physical therapy. If these are ineffectual, spinal implants are recommended. [57] The number of surgical procedures in the treatment of symptomatic DDD is increasing. However, the effectiveness of surgery has not had only convincing evidence. [58]

6.1 Anatomy of the spine

The function of the spinal column is to protect the spinal cord and to be a connection to the central nervous system. The spinal column comprises 33 individual bones called vertebrae that are divided into three groups: cervical, thoracic and lumbar vertebrae (Figure 21). The sacrum comprises 4-5 fused bones and the tailbone (coccyx) contains 3-5 fused bones. The cervical region (C1-C7) enables the rotation of the neck and the movement of the head. The thoracic vertebrae (T1-T12) house the rib case and assists the motion of bending, twisting, and side extension. Lumbar spine (L1-L5) provides support of the body weight in sitting or standing. The sacrum functions as the foundation of the pelvis. The sacrum and the coccyx together support and balance upright body. [1]

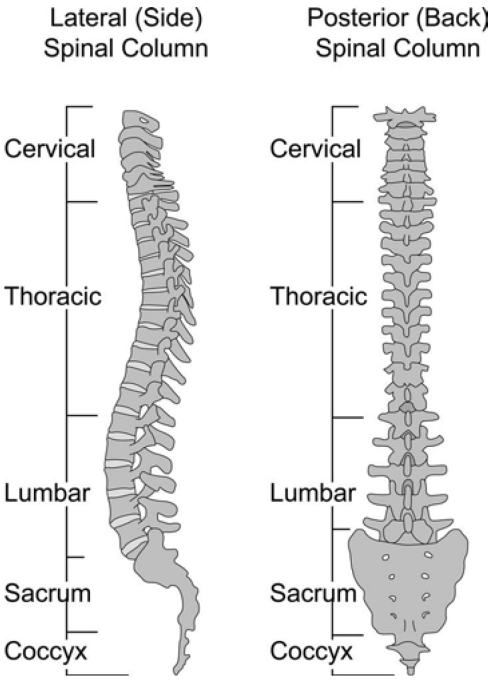

Figure 21. The anatomy of a healthy spine. [1]

The vertebrae are separated by intervertebral discs that absorb shocks (Figure 22). The outer layer of disc is called the annulus, which protects the soft viscoelastic interior, the nucleus. The nucleus has several functions: bearing the axial loads of the spine, providing a pivot point for torsional movement of the lower body and attaching the vertebrae together. [1] The healthy disc allows also bending, flexion and torsion of the spine. Altogether the discs make up about one third of the spinal length.[59]

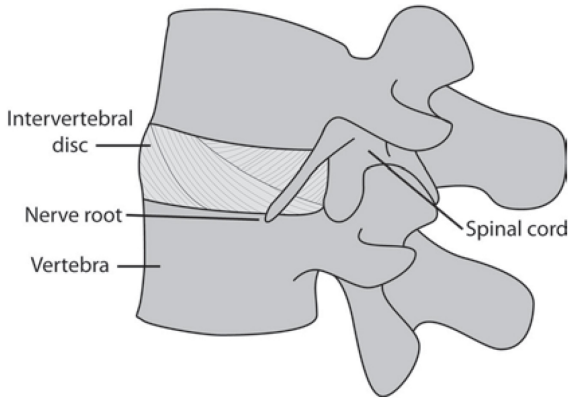

Figure 22. Intervertebral disc between vertebrae. [1]

6.2 Challenges with spinal implants

As with any medical device, the spinal implants have to be biocompatible, offer resistance to wear and fatigue damage, and withstand loading. There are six degrees of freedom in the kinematics of spine, including flexion-extension, lateral flexion, and axial rotation. Therefore, in addition to compressive and tensile axial strength, the implant must offer also flexural strength and torsional strength. Also, the position in the spine affects greatly on the loads and strains. These factors also make the design of implants extraordinarily challenging. The complex biomechanics of the spine is illustrated in Figure 23. [1]

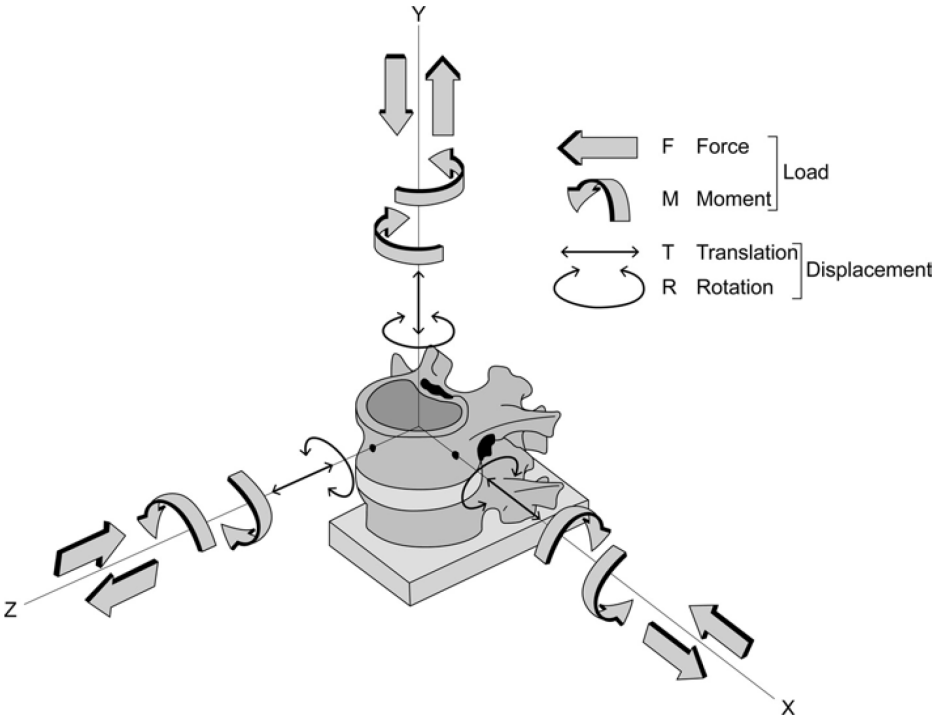

Figure 23. Biomechanics of the spine. [1]

In comparison to general orthopedics, the spinal implant's situation in the spine is more difficult when dealing with infection. A spinal infection is difficult to treat and an infection in the presence of an implant is even more difficult. This is due to the anatomical position of the implant as well as the difficulty and risks of revision approaches [60]. Therefore, infections should be prevented instead of treating them. Methods to prevent infections are including antibiotic prophylaxis (preventive medication), surgical technique to avoid necrotic tissue, reduction of haematomas, optimizing surgical conditions and treating co-existing infections. There is a

consensus that patients should receive antibiotics before the spine surgery. [61] In addition, some patient groups make spinal implantation challenging, such as smokers, patients with multiple past surgeries, and patients with poor bone quality [62].

6.3 Present state of spinal implants

There are two types of medical devices used in the spine. The first type of device are those that lead to fusion of two or more vertebra [63]. Spinal fixation (spinal fusion) is a method where the fractured spine is stabilized with screws and plates or rods. Also wire and bone grafts have been used to spinal fixation. Contemporary spinal fixation is made with screws and rods [64]. Spinal fusion is the ”gold standard” for treatment of degenerated intervertebral discs [59]. It is also the most popular surgical operation in spine [57]. In spinal fusion, the degenerated intervertebral disc is removed and the vertebral bodies are fused [59]. The removal of intervertebral disc is called discectomy [57].

The second type is a disc replacement where a damaged or diseased disc is removed and replaced with an implant. [1] Unlike spinal fusion methods, artificial total disc replacement (TDR) is designed to restore the segmental motion of the spine or to give back some of the motional freedom. Currently used implants have only medium outcome success and have relatively high re-operation rates. [59] It is still uncertain if TDR is more effective and safer than fusion [65].

6.3.1 Disc replacement implants

There are several disc replacement implants. Lumbar spine implants are different compared to implants in cervical spine due to different biomechanical requirements. This literature review focuses on recent lumbar intervertebral implants.

The Charite™ has been a widely used lumbar intervertebral implant. The core is ultra-high molecular weight polyethylene (UHMWPE) and the endplates are made of cobalt-chrome (Co-Cr) alloy (Figure 24). UHMWPE acts as mobile unit allowing the normal motion of the spine. [1] The Charite™ disc has been taken off the market

because of the poor sales, even though it had a lifetime of over a quarter of a century [66].

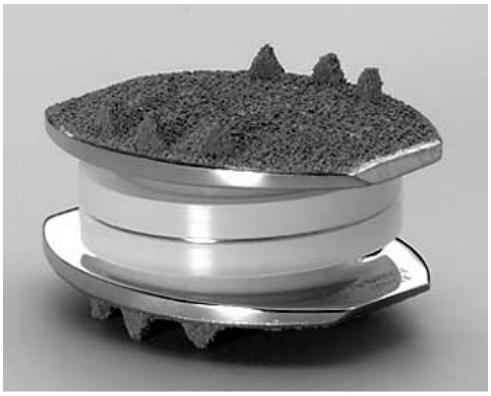

Figure 24. The Charite™ lumbar intervertebral implant. [67]

The Pro-Disc™ consists also of CoCr alloy and UHMWPE. The implant utilizes metal-on-plastic bearing coupling. [1] Figure 25 shows the assembled Pro-Disc™ that consists of three components. The problem with both metal-on-plastic implants is polymer wear, subsidence and migration, even though both Charite™ and Pro-Disc™ are successful implants. [1] The Pro-Disc™ is the only commercially available disc prosthesis in the United States, because Charite™ is not available anymore [66].

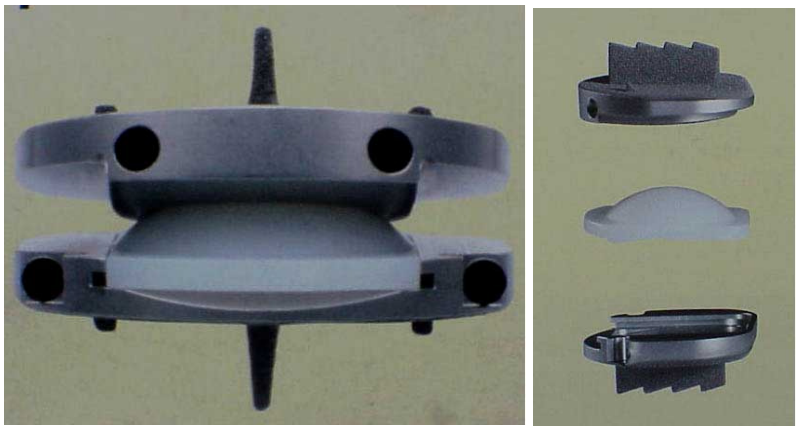

Figure 25. The Pro-Disc™ intervertebral implant. [68]

Maverick™ implant is made of CoCr alloy and it is a metal-on-metal implant. The implant has a fixed posterior center of rotation, which mimics the kinematics of the intervertebral motion. [1] Figure 26 shows the Maverick™ implant. The Maverick™ total disc replacement implant has been used in Europe and Australia, but is not yet FDA (U.S. Food and Drug Administration) approved in United States. Metal-on-metal surface might cause metal wear which results in a significant host reaction [66].

Figure 26 The Maverick™ implant. [69]

The Flexicore™ implant is also made of CoCr. A ball-and-socket joint links the superior and inferior endplates. The endplates are dome shaped and there is a rotational stop and a tension bearing. These features prevent the separation or dislocation of the endplates. [1] Flexicore's preliminary trial results did not show clinical relevant differences between TDR surgery and fusion techniques. Even though the authors reported decreased pain intensity and a slightly better functional impairment in Flexicore group than in the fusion group, the statistical significance was not reported. [58] The Flexicore™ implant is shown in Figure 27.

Figure 27. The Flexicore™ implant. [68]

In addition to Maverick™, Chartie™, Pro-Disc™ and Flexicore™, there are also other lumbar TDRs under investigation and emerging to market, such as Mobidisc, XL TDR, Freedom lumbar disc, Activ-L, Kineflex and Triumph. [63] Figure 28 shows the designs of the lumbar disc replacement TDRs not yet in market.

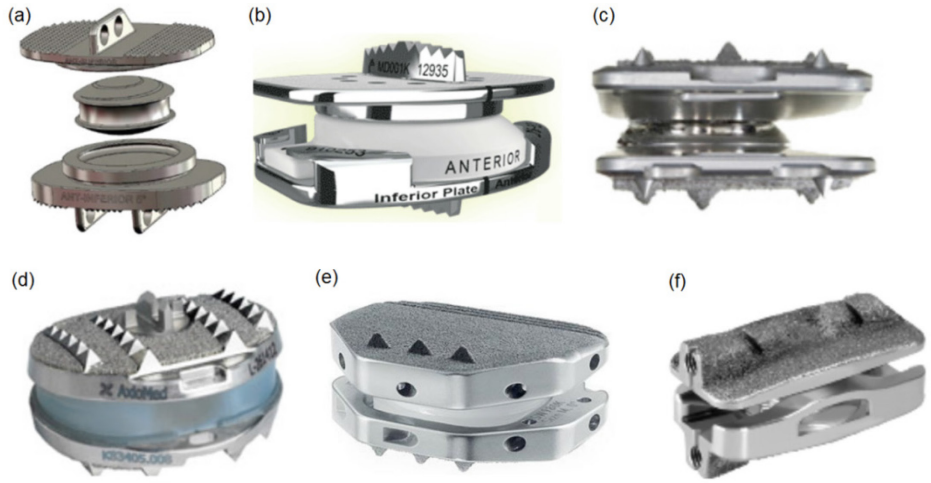

Figure 28. Lumbar TDRs. (a) Kineflex; (b) Mobidisc; (c) XL TDR; (d) Freedom; (e) Activ-L; and (h) Triumph. Modified [63]

6.3.2 Cages

Interbody cages and vertebral body replacements enable the bone healing across a previously mobile motion segment. Some cages are intended to contain bone graft or an osteogenic substance. [63] Autograft is the “gold standard” for spinal fusion. Anterior lumbar interbody fusion (ALIF) has become one of the primary choices for eliminating motion between vertebrae. [62] Also other surgical techniques are used, such as transforaminal lumbar interbody fusion (TLIF) and posterior lumbar interbody fusion (PLIF).

Interbody cages are used between two vertebrae. Their purpose is to restore lost disc height and relieve back pain. There are numerous interbody cage models and retailers.

Titan Spine offers a titanium Endoskeleton® interbody fusion devices. They have devices for different surgical techniques. [70] Trabecular Metal™ Material from

Zimmer is made of tantalum. It is highly porous, structural biomaterial, which promises rapid, substantial bone ingrowth [71]. DePuy Syntes has several interbody cage products such as Polyetheretherketone (PEEK) vertebral spacer and titanium alloy (Ti-6Al-7Nb) SynCage Spacer [72]. Spine Craft offers ORIO-AL ALIF PEEK-Optima® Cage [73]. ALIF PEEK cage from BM Korea Co. is made also from PEEK-OPTIMA™ material [74]. Figure 29 shows pictures of presented implants.

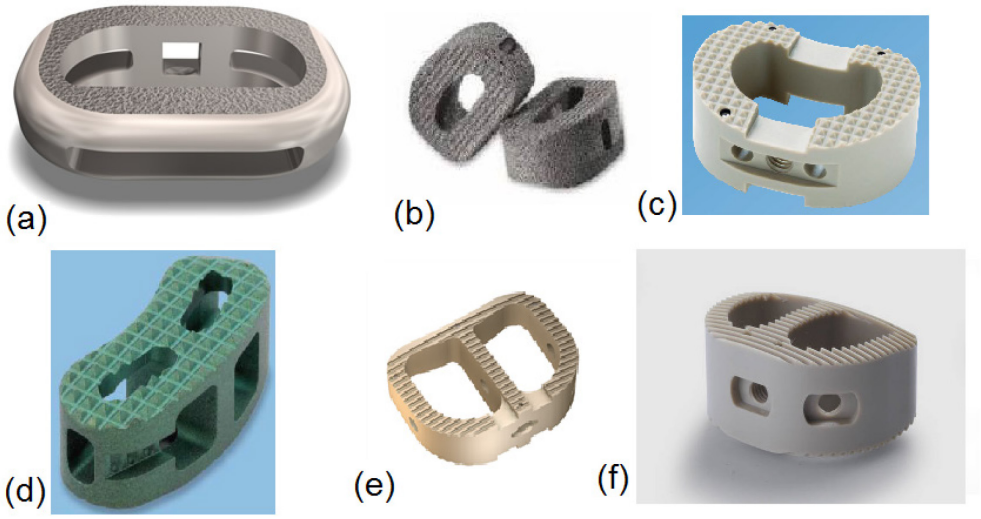

Figure 29. Interbody cages. (a) Endoskeleton® [70]; (b) Trabecular Metal™ Material ALIF Device [71]; (c) PEEK vertebral spacer [72]; (d) SynCage Spacer curved [72]; (e) ORIO-AL ALIF PEEK-Optima® Cage [73]; (f) ALIF PEEK cage [74].

The MOSS titanium mesh cage ("Harms mesh cage") and Synex™ cage are vertebral body replacement devices (Figure 30). MOSS has been used successfully for 25 years. It was developed in 1986 and the technology is relatively simple. Cylindrical shape titanium mesh has reinforcement rings at each end. This is a stable structure which is filled with bone graft before implantation. The primary filler is autograft. There are different sizes of MOSS cages. [62] Syntex is newer vertebral body replacement device. Its height is adjustable and it is extended *in situ* to the required size. [75]

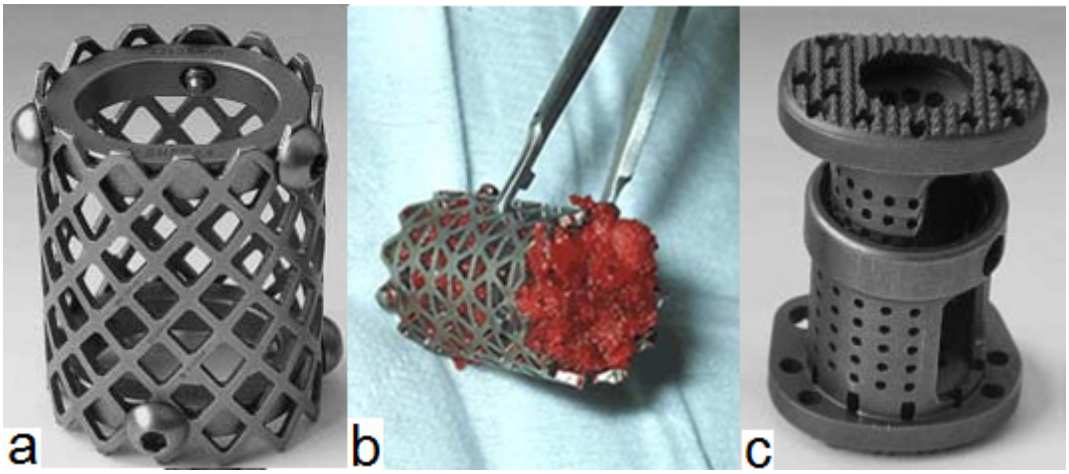

Figure 30. (a) MOSS vertebral body replacement. [76]. (b) Titanium Mesh Cage packed with autogenous trabecular bone resected from the fracture site, [77] modified. (c) Synex^{TM} [76]

7 Scope of the research

The target of this thesis was to investigate preparation of 3D bioactive titanium/polymer hybrid materials. The primary target was the preparation of hybrid material combining titanium mesh and porous biodegradable polymer matrix. In addition, filling titanium mesh with crushed bone graft was investigated.

The planned application area for titanium/polymer hybrid materials is orthopedic implants. The goal was to manufacture materials that have proper mechanical properties for load-bearing applications. The materials should also have a suitable porous structure for cell ingrowth and be bioactive to induce osteogenesis. The role of titanium is to function as a load-bearing component, whereas the polymer matrix offers a suitable porous structure for cell-ingrowth and a matrix for bioactive glass (BAG) to induce osteogenesis.

In this study different methods to prepare titanium/polymer hybrid materials were studied. The used biodegradable polymer was PCL because it is one of the polymers that are FDA approved. Therefore it can enter to clinical stage remarkably faster compared to a new polymer without FDA approval. Both photo-crosslinkable and thermoplastic PCL were used. Cross-linkable PCL oligomers were synthetized from ε-caprolactone and methacrylated whereas thermoplastic PCL was used as received.

Porous PCL was prepared by salt leaching method from photo-crosslinkable methacrylated oligomers. Salt leaching was used because it is easily performed method and with the used salt calcium chloride hexahydrate ($CaCl_2 \cdot 6\ H_2O$) the pores formed have a suitable pore size and they are interconnected [78]. However, with salt leaching there is always a possibility that part of the salt remains in the polymer matrix especially with larger samples. Therefore, other methods to prepare porous samples were used with thermoplastic PCL. These are freeze extraction, freeze drying and dipping. There is no concern with unwanted chemicals in the complete sample, because the solvents used in these methods evaporate.

Scanning electron microscope (SEM) and micro computed tomography (μCT) were used to analyze the pore size and porosity of freeze extraction samples. μCT was

used also with titanium mesh samples filled with crushed bone to determine the consistence of filling.

The load-bearing capacity of the prepared samples is an important aspect when considering the application area in orthopedics. Therefore, compression testing was performed for the samples containing titanium or bone, as well as PCL and PCL+BAG samples prepared by crosslinking.

8 Materials

The polymer used in this research was polycaprolactone (PCL). Both photo-crosslinkable polycaprolactone oligomer and thermoplastic polycaprolactone were used. Thermoplastic polycaprolactone was provided by Purac Biomaterials. PCL was dissolved into 1,4-Dioxane (Sigma-Aldrich Chemie, Germany) for the freeze extraction and coating process. For the freeze drying process, chloroform (Merck Chemicals, Germany) was used.

Star-shaped polycaprolactone oligomers were synthetized from ε-caprolactone (CL, Sigma-Aldrich Chemie, USA) using stannous(II)2-ethylhexanoate ($Sn(Oct)_2$) as an initiator (Sigma-Aldrich Chemie, Germany) and pentaerythritol (PERYT, Sigma-Aldrich Chemie, Germany) as a co-initiator. Methacrylic anhydride (MAAH, Sigma-Aldrich Chemie, Germany) was used for the functionalization. Camphorquinone (CQ, Sigma-Aldrich Chemie, Germany) was used as the photo-initiator for the photopolymerization of functionalized polycaprolactone oligomers. All chemicals were used as received.

Bioactive glass (S53P4, Vivoxid LTd, Finland) was used as a bioactive component in polymer matrixes. S53P4 is a mixture of CaO, Na_2O, P_2O_5, and SiO_2. The particle size used in this study was ≤ 40 mm. For making porous polymer structures by salt leaching, calcium chloride hexahydrate ($CaCl_2 \cdot 6\ H_2O$, Sigma-Aldrich Chemie, Croatia) was sieved to obtain appropriate size crystals. Chloroform-d (Euriso-top, France) was used for nuclear magnetic resonance (NMR) measurements.

The titanium alloy networks were ordered from a German company FIT Fruth Innovative Technologien GmbH. The networks were made by EBM process. The alloy powder used was $TiAl_6V_4$ extra low interstitial (Ti64 ELI) which is highly resistant to corrosion and biomedically compatible. The manufacturer promises titanium structure to be 100 % dense. [45]

Eero Huotilainen from Business, Innovation, Technology (BIT) research unit of the Department of Industrial Engineering and Management, Aalto University School of Science designed the structure of titanium networks. Networks for cages were designed according to the dimensions given by Professor Petri Lehenkari from University of Oulu. The networks are presented in Figure 31 and Figure 32. The dimensions for mesh were following: width 40 mm, depth 30 mm, front height 15 mm

and back height 8 mm. The angle between front and back is 12 º. Dimensions of struts were selected to have a thickness of 1 mm and length of 4 mm. Pretests have shown that these dimensions allow the network to be filled with polymer. The structure was chosen to be diamond cubic crystal structure. The networks for compression tests were selected to be cylinders (Figure 33) with height 15 mm and diameter 14 mm. The general structure of the networks is similar for both meshes.

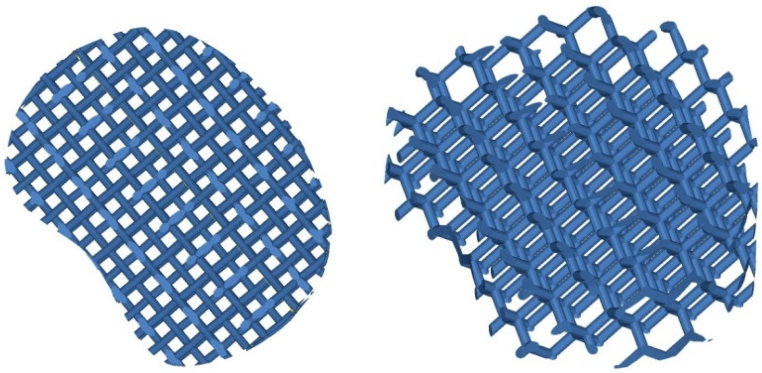

Figure 31. Design of cage implant. Images received from BIT.

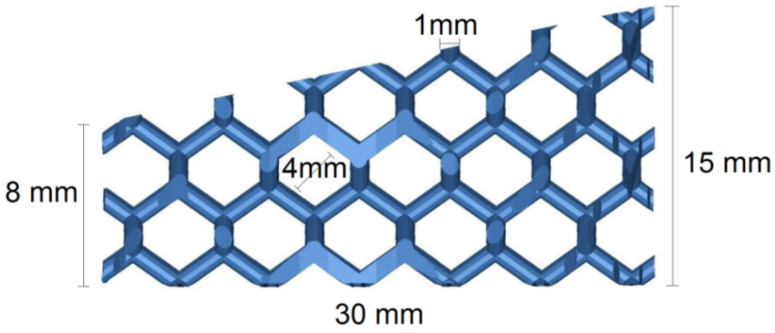

Figure 32. Design of cage implant from side. Image received from BIT, modified.

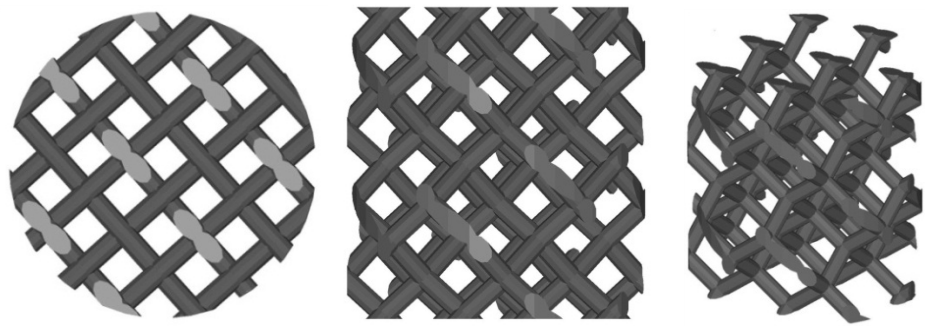

Figure 33. Design of cylinder network. Images received from BIT.

The porosity of cylindrical networks was determined by comparing the weight of the porous implant with the theoretical weight of solid sample with the same dimension and density. The density of solid $TiAl_6V_4$ is 4.43 g/cm^3. [36] The volume of cylindrical networks was 3.02 cm^3. The weight of a solid sample should thus be 13.38 g. The average weight of cylindrical mesh was 0.79 g. The weight of cylindrical mesh was 6 % of the weight of solid cylindrical piece. Therefore, the porosity of meshes was approximately 94 % and the bulk density was 0.26 g/cm^3.

9 Methods

Four different methods were used to manufacture porous polymer matrices from cross-linkable PCL oligomers and thermoplastic PCL. To prepare cylinder shaped samples for compression testing, Teflon molds were used. The diameter for a mold was 17 mm and height 20 mm. A top side and a bottom side of the mold are open. The same molds were used also for samples with thermoplastic PCL. In addition to PCL samples, titanium mesh was filled with crushed bone graft.

9.1 Preparation of cross-linked polycaprolactone samples

The polycaprolactone oligomers were synthesized using bulk ring-opening polymerization described earlier [79]. The polycaprolactone oligomers were polymerized in a batch reactor at 160 ºC under a nitrogen atmosphere. The ε-caprolactone monomer was fed into the reactor with appropriate amount of PERYT for 1 h to dissolve the co-initiator into the monomer. The initiator $Sn(Oct)_2$ (0,02 mol-%) was added and the polymerization was continued for 5 h.

The co-initiator affects the structure of the polymer and increases the reaction rate of polymerization. PERYT is a symmetrical star-shaped molecule which has 4 functional OH-groups in equivalent positions. Therefore it yields 4-arm polymers. The amount of PERYT affects the molar mass of oligomer. [79] As oligomers with low viscosity were preferred, high amounts of PERYT were needed. For the chosen amount of PERYT, 12 mol-% in respect of the monomer amount, theoretical molar mass is 1087 g/mol. The chemical reaction of the preparation of oligomers is presented in Figure 34.

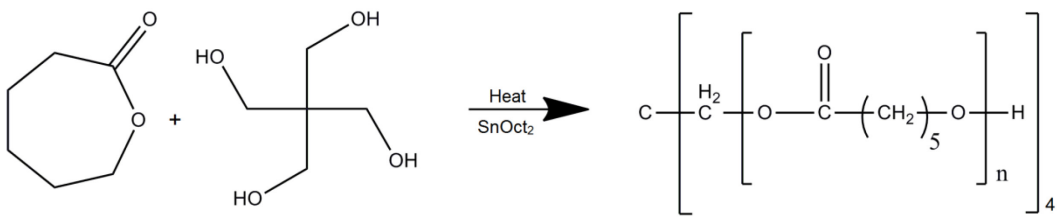

Figure 34. The reaction scheme of ring-opening oligomerization of ε-caprolactone. Modified [80].

After the synthetization, the hydroxyl end groups were methacrylated with MAAH. The functionalization was carried out in a batch reactor at 60 ºC for 24 h. The chemical reaction of functionalizing oligomers with methacrylic anhydride is presented in Figure 35.

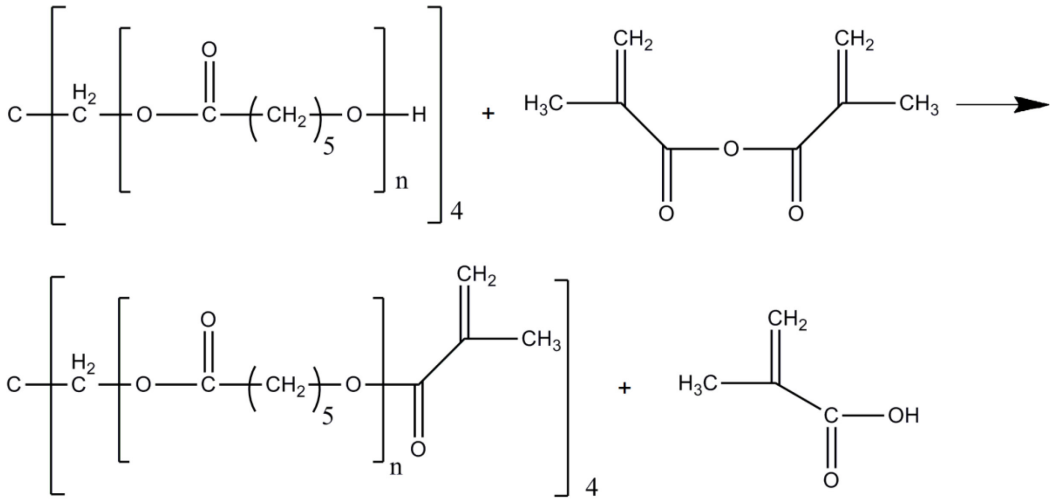

Figure 35. The reaction scheme of functionalization with methacrylic anhydride. Modified [80].

Functionalized polymers were isolated by the precipitation of the reaction mixture in n-hexane. The precipitation was made 10 consecutive times. Hexane was mixed with magnetic stirrer in room temperature with reaction mixture and precipitation was carried out in ice bath. Finally, methacrylated oligomers were dried in vacuum.

For crosslinking, 1 w-% CQ was added to methacrylated oligomer and stirred with spatula. The mixture was left under an aluminum cup for 1h. Aluminum prevents light access to the mixture and avoids light induced crosslinking. The procedure dissolves CQ more efficiently and a more homogenous mixture is received. The next step was to add bioactive glass (20 w-% of polymer) and/or $CaCl_2 \cdot 6\ H_2O$ (67.6 w-% of PCL-BAG composite). Finally, the mixture was poured into Teflon molds which were placed on silicone coated polyethylene terephthalate (PET) films (Votafilm® 2645, Isovolta AG, Austria) and metal plates to ease the transferring of molds. In case of titanium mesh, the mold was first filled halfway with polymer mixture. Second, mesh was filled with polymer paste. Thirdly, titanium mesh was pushed to

the mixture. Finally, mold was filled full. Filled molds were allowed to rest under aluminum cups for minimum 1 h to remove air bubbles from the polymer mixture.

Filled molds were covered with silicone coated PET film and placed into the Triad® 2000 light curing system (DENTSPLY, Canada). First, both sides were cured two times for two minutes and after that the films were removed. Second, both sides were cured for six minutes and samples were removed from the mold. Finally, both sides of samples were cured six minutes three consecutive times. In total, both sides were cured for 28 minutes.

When $CaCl_2 \cdot 6\ H_2O$ was used, the remaining salt had to be removed with ethanol. The skin of the samples was removed with sharp blade. A beaker was filled with ethanol and a magnetic stirrer was placed on the bottom. A rack was placed into ethanol so that the magnetic stirrer could rotate freely. Samples were placed to the rack allowing the whirling ethanol to rinse the $CaCl_2 \cdot 6\ H_2O$ out of the samples for four days. After salt was removed, the samples were dried in vacuum for one day. Abbreviations for the samples are presented in Table 4 and picture of samples is in Figure 36.

Table 4. Abbreviations for photo-crosslinked PCL samples.

Abbreviation	bioactive glass	titanium mesh	porous
PCL			
p-PCL			x
PCL-BAG	x		
p-PCL-BAG-titanium	x	x	x

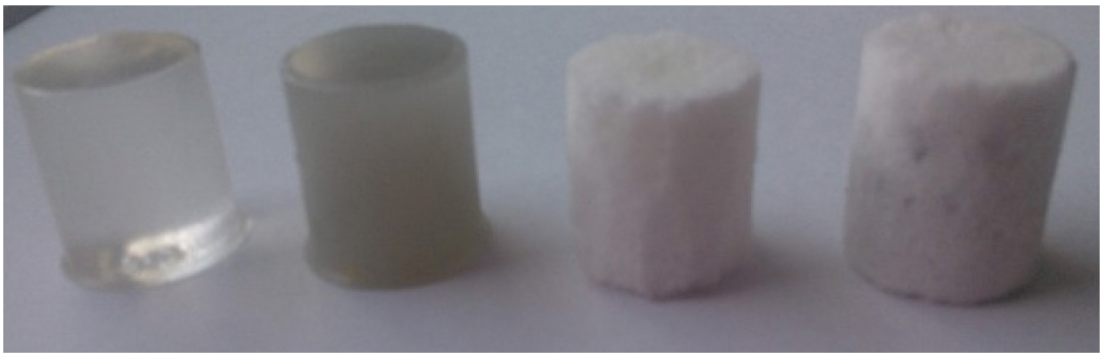

Figure 36. Samples for compression testing. From right: PCL, PCL-BAG, p-PCL and p-PCL-BAG-titanium.

Weights of samples were measured before curing and when the samples were finished. Also the removed polymer skin was weighted. It was assumed, that polymer skin contains only PCL and BAG. $CaCl_2 \cdot 6\ H_2O$ could not be removed totally from the polymer matrix. Approximately 83 w-% of $CaCl_2 \cdot 6\ H_2O$ was dissolved. Therefore, the porosity of the samples was approximately 49.4 vol % instead of the theoretical 59.5 vol %. The effect of titanium meshes to the porosity is not approximated.

9.2 Preparation of thermoplastic polycaprolactone samples

Freeze extraction, freeze drying and dipping methods were also tried to manufacture porous polymer samples and polymer coated titanium meshes. Thermoplastic PCL was used in these methods.

9.2.1 Freeze extraction

Freeze extraction is a method to manufacture porous polymer structures. It has been used for example in manufacturing porous membranes of PLLA/PCL solutions [81,82] and of titanium/ biodegradable polymer (PLLA) scaffolds with microporous polymer structure [55]. Freeze extraction is a thermally induced phase separation technique. The pores are formed via extraction of the frozen solvent from frozen polymer solution via non-solvent for the polymer. The technique has several advantages: it does not have residual solvent problem, is easy to scale up, and forms open, interconnected pores. Molds can be used to direct the process to form pore gradients to control cell migration. [55] On the other hand the pores are small; 5-10 µm [82].

PCL (0.26 g) was dissolved into 1,4-dioxane (5 g) with a magnetic stirrer. This should yield approximately 95 % porosity. When bioactive glass (0.04 g) was used, it was added immediately before freezing the samples. The Teflon mold was attached to a plastic petri dish with freezing distilled water in freezer at -22 ºC. Polymer solution was poured into the mold and silicone coated PET film was placed on the mold. For the samples prepared for SEM, in the case of bioactive glass and polymer solution, the mold was freeze also with liquid nitrogen before pouring the

solution. This is because μCT images revealed bioactive glass to be sunk to the bottom of the sample. Therefore, faster freezing should be used to avoid high concentrations of bioactive glass on the bottom.

After 2 hours in the freezer, the samples were detached from the petri dish. The samples were placed in beakers filled with – 10 ºC ethanol. The beakers were placed on a rack in thermostat (RM 6 B, Lauda, Germany). The thermostat was filled with deionized water – monoethylene glycol mixture (HD Zero BS6580, The Aspo Company, Finland) with ratio 1:1 and the temperature of the mixture was adjusted to be -10 ºC. The samples were immersed in ethanol for 2 d 19 h.

After the immersion in ethanol, the samples were removed and placed in a fume hood to allow ethanol to evaporate for 1 d. Finally, the samples were dried in vacuum overnight. The abbreviations for the samples are following: the PCL sample is PCL and the PCL sample with bioactive glass is PCL-BAG.

The scaffolds obtained by the described method were highly porous and soft. They had a hole in the middle on the top of the sample. They do not have suitable mechanical properties for load-bearing applications. Therefore the scaffold made with this technique needs a load-bearing matrix, such as titanium mesh.

Lebourg *et al.* [81] and Gaona *et al.* [82] prepared solutions of mixes of PCL and PCL/PLLA blends in different weight ratios. All polymer-dioxane solutions were frozen in liquid nitrogen. Freezing the solutions with liquid nitrogen was also tried. However, that did not freeze the sample fast enough and part of the solution drained out of the mold. This yielded un-uniform samples.

Vrana *et al.* [55] dissolved PLLA in dioxane-water binary mixture and froze the samples at -80 ºC. Dioxane-water binary mixture was tried in this study. There was no possibility to freeze samples in -80 ºC. Therefore, the samples were frozen with liquid nitrogen or in freezer at -22 ºC. Liquid nitrogen yielded to bursting of the solution out of the mold. In the freezer, big holes emerged during freezing. Therefore, freezing samples with liquid nitrogen and using dioxane-water mixture was not considered a success. However, if compared to freezing at -22 ºC faster freezing at lower temperature might be affordable in preventing holes in the samples.

9.2.2 Freeze Drying

Freeze drying can be used to manufacture porous polymer structures. It is also based on phase separation technique, in which phase separation of homogenous biodegradable polymer solution occurs due to a lowered temperature. Using temperature which freezes the solution, the phase separation mechanism is solid-liquid demixing. That forms frozen solvent and concentrated polymer phases. The frozen solvent is removed and pores are formed into spaces that were originally occupied by the solvent. The morphology of prepared porous structure is adjusted by polymer concentration, solvent and cooling rate. These factors affect to the mechanism of phase separation and thus pore structure formation. [83]

2 g PCL was dissolved into 10 ml chloroform in room temperature. The Teflon mold was attached to a plastic petri dish with freezing distilled water in freezer at -22 ºC. PCL solution was poured into the mold and liquid nitrogen was poured outside the mold. The solution started to freeze from the borders of the mold and small hole appeared on the center of the sample.

The frozen sample was placed in a freeze dryer (Zree Zone -105 ºC 4.5 Liter Cascade Benchtop Freeze Dry system, Labconco, USA) and dried in vacuum for 4 h 30 min. Polymer was erupted from the center of the sample (Figure 37).

Figure 37. Sample prepared by freeze drying.

9.2.3 Dipping

PCL was dissolved in chloroform to obtain a solution with suitable viscosity for dipping. To dissolve PCL, a magnetic stirrer was used. A suitable viscosity was received when 5 g PCL was dissolved in 30 ml chloroform.

The titanium mesh was dipped in polymer solution. The solution formed membranes between edges. These membranes were broken with gaseous nitrogen flow. The dipping was made three consecutive times to achieve uniform coating. After every dipping, the solvent was allowed to evaporate for minimum 20 minutes before new dipping.

The dipping was also tested with 20 w-% of bioactive glass. Bioactive glass was added to polymer solution and mixed with magnetic stirrer. The bioactive glass blended well with the solution, but sunk after a while to the bottom of the beaker. Therefore, the solution had to be stirred before every dipping. A suitable number of dipping in this case was three to four times.

9.3 Preparation of titanium-bone graft samples

Titanium-bone graft samples were prepared at University of Oulu at the Department of Anatomy and Cell Biology. The bone graft is bone received from a patient. The blood and bone marrow are removed from the bone graft. The bone graft had been crushed and stored at 80 % ethanol in refrigerator.

The titanium mesh was cleaned with Digital ultrasonic cleaner (SS-802, ProsKit, USA). The ultrasonic cleaner was filled with distilled water and titanium meshes were cleaned in the ultrasonic cleaner for 7 min and 50 s.

The titanium networks were filled up with crushed bone. Tweezers and pestle were used as tools in filling. The filling of titanium mesh with crushed bone took quite a long time, because the bone was hard to get inside the mesh. Smaller bone pieces would have been easier to be used in filling. Figure 38 shows the filling process.

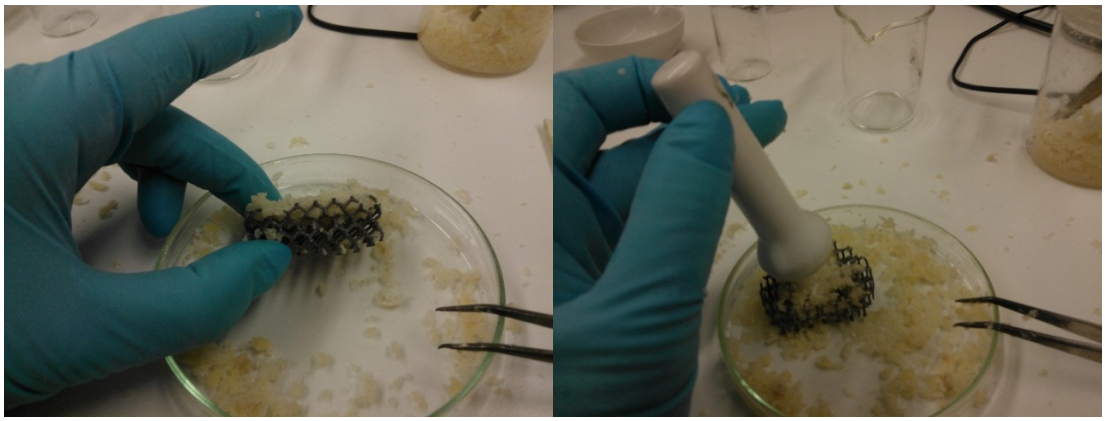

Figure 38. Filling of titanium mesh. Right: Mesh could be filled from other side only to half way. Left: Tweezers and pestle was used in filling.

10 Results and discussion

10.1 Characterization of cross-linkable polycaprolactone samples

The structure of polymers was determined using a Bruker Ultrashield 400 Hz NMR spectrometer (Billerica, MA, USA). The samples (5-10 mg) for ^{1}H measurements were dissolved in 0.5 ml d-chloroform (99.8 % deuteration). The measurements were performed at 25 ºC.

PCL oligomers were polymerized in bulk using $SnOct_2$ as the initiator and PERYT as the co-initiator to produce star-shaped low molecular weight oligomers. The monomer conversion was complete as no monomer peak (2.66 ppm) was observed in ^{1}H-NMR spectrographs. The methacrylation was complete as OH end groups (peaks 3.65 ppm and 3.50 ppm) were not observed. Figures 39 and 40 show the the 1H-NMR spectras of PCL oligomers before and after methacrylation, respectively.

Figure 39. ^{1}H-NMR of OH-terminated PCL oligomer.

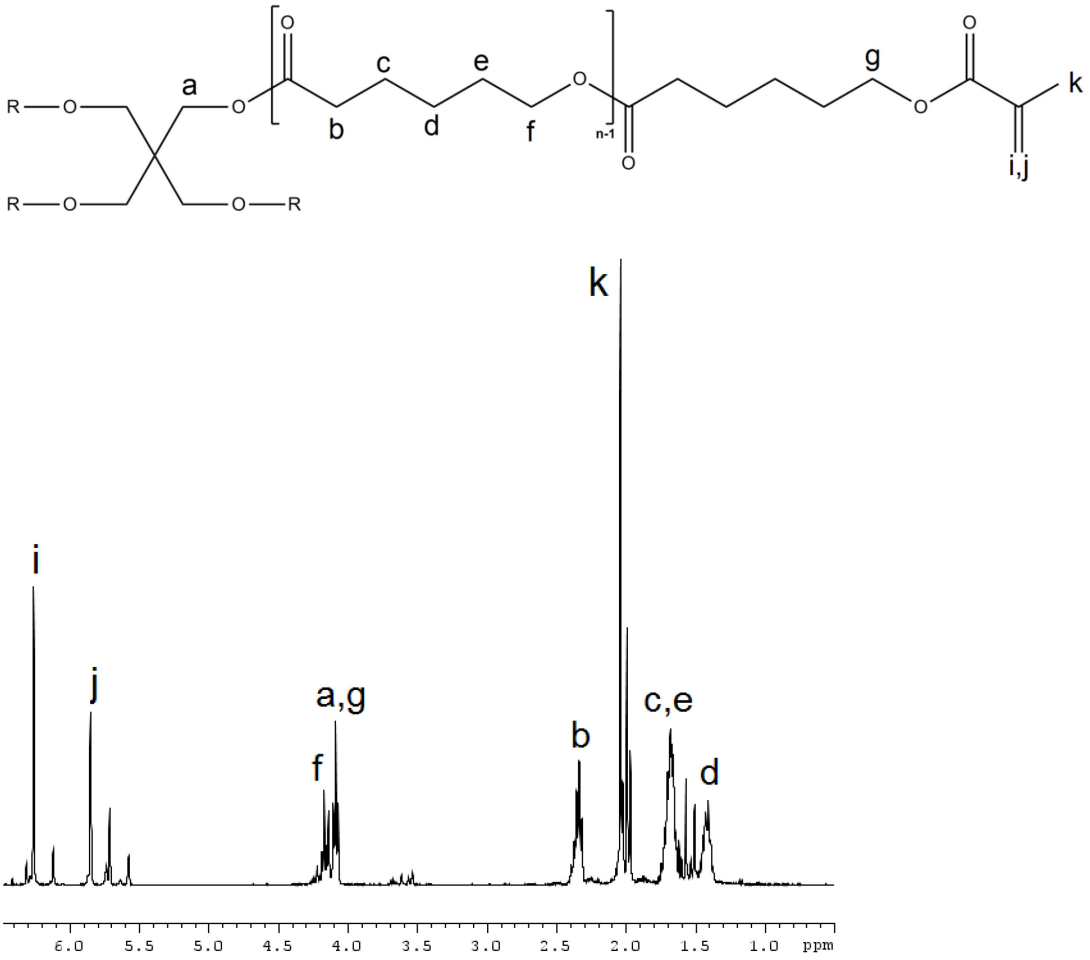

Figure 40. ^{1}H-NMR of methacrylated PCL oligomer.

10.2 Size-exclusion chromatography

Waters (Milford, MA, USA) size-exclusion chromatography (SEC) was used to analyze the number average molecular weight (M_n) and polydispersity indexes (PDIs) of different PCL samples. The Waters SEC system consists of a Waters 717plus autosampler, a Waters 510 HPLC pump and a Waters 2414 refractive index detector and columns involved in molecular weight separation. Chloroform was used as eluent. The results were processed with the Empower software by Waters using narrow molecular weight polystyrene calibration. The samples (10 mg) were dissolved in chloroform (10 ml) before the analysis.

Table 5. shows results for relative molar masses and PDIs for samples. Three batches of methacrylated PCL oligomers were prepared. These are denoted as PCL I, PCL II and PCL III.

Table 5. Relative molar masses of thermoplastic PCL and different metharylated oligomer samples.

Sample	M_n (g/mol)	PDI
Thermoplastic PCL	69600	1.8
Methacrylated PCL oligomers		
PCL I	2800	1.2
PCL II	3000	1.1
PCL III	3100	1.2

10.3 Determination of gel content

The gel content is the insoluble fraction which is produced by crosslinking. The gel content can be determined by extracting polymer with solvents. The determination of gel content was made for photo-crosslinked PCL samples. The samples have been in compression testing. The cross-linked PCL was taken from the middle of the compression specimen to determine the crosslinking in the middle of the samples. Before testing, the samples had been kept in vacuum for two days to remove moisture.

Specimens were prepared by cutting a rectangle piece of 120-mesh stainless steel cloth. The mesh was folded to form a square. Two sides of this square are closed by folding the cloth at the edges to obtain a pouch open at the top. The pouch is weighted. Approximately 0.1 mg of the PCL is weighted and placed in the weighted pouch. The open side of pouch is folded over to form a cage. The total weight of PCL and the pouch is calculated. Three samples were prepared.

A Soxhlet extractor was used in the determination. A round-bottom flask (500 ml) was filled with 350 ml acetone. Acetone was heated to boiling point and the samples were placed in the thimble. The samples were extracted for 20 hours in acetone. After extraction, the samples were placed in vacuum for 13 h. Cage and PCL were weighted and gel content was calculated. The average gel content for the samples was 99.88 %.

10.4 Compression testing

Compression testing was performed using Instron 4204 (Instron, USA) apparatus. The software used was Bluehill 2 (Instron, USA). Six kinds of specimens were prepared: solid PCL, porous PCL, solid PCL-BAG composite, porous PCL-BAG-titanium mesh hybrid material, titanium mesh and titanium mesh filled with bone graft. The amount of samples was three for all sample groups. All the PCL samples were prepared by photo-crosslinking of methacrylated PCL oligomers. The shape of the tested specimens was cylindrical. The specimens were prepared using the same Teflon mold with diameter 17 mm and height 20 mm. However, the sizes of the finished specimens varied slightly. Firstly, this is due to the fact that the titanium meshes had to be a bit smaller compared to the mold so that they could fit in. Secondly, porous PCL samples (p-PCL and p-PCL-BAG-titanium) prepared by crosslinking methacrylated PCL oligomers had a polymer skin on the surface. The skin had to be removed before dissolving the $CaCl_2 \cdot 6\ H_2O$ in order to promote the salt leaching process.

The testing was done at 23 ºC and 50 % humidity. The testing speed was 1 mm/min. 5 kN load was used to porous samples and samples with titanium meshes. 5 kN load was not enough for solid PCL and PCL-BAG samples. Therefore, 50 kN load was used for these samples. The compressive modulus and compressive stress and strain at yield were calculated. The means and standard deviations were calculated from the results.

Figure 41 and Figure 42 show the compression stress-strain curves for samples containing titanium mesh. The samples have similar compressive stress values regardless of bone or polymer matrix filling. The curves in Figure 41 have similar shape. The titanium-bone sample has some crushed bone on the top and the bottom of the sample. The curve shows first how crushed bone moves and compresses before close contact between the titanium and compression plates. There was only one titanium-bone sample. Therefore no further conclusions about the effect of the bone graft on compressive stress can be made. Figure 41 shows also how titanium mesh starts to break one strut at a time after the compression stress at break. The breaking pattern was similar for all the titanium mesh samples.

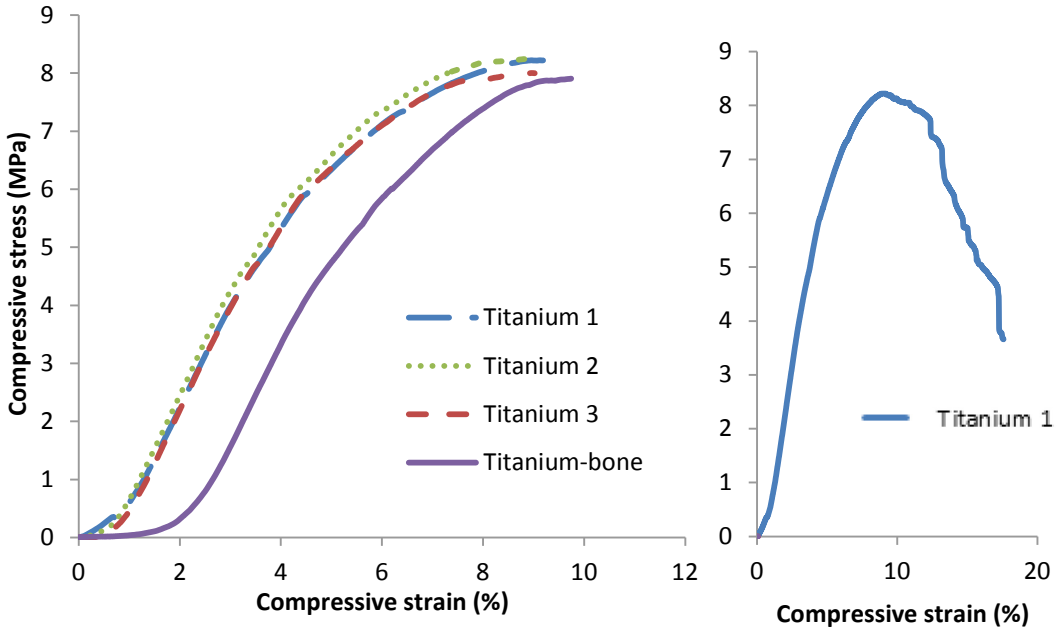

Figure 41. Compression stress-strain curves for titanium meshes and titanium-bone sample.

Figure 42 shows the curves for p-PCL-BAG-titanium samples. The p-PCL-BAG-titanium samples have different curve shape in the beginning of testing compared to titanium mesh samples. It is due to the polymer that is first compressed. As the testing is continued, the titanium mesh begins to affect the result.

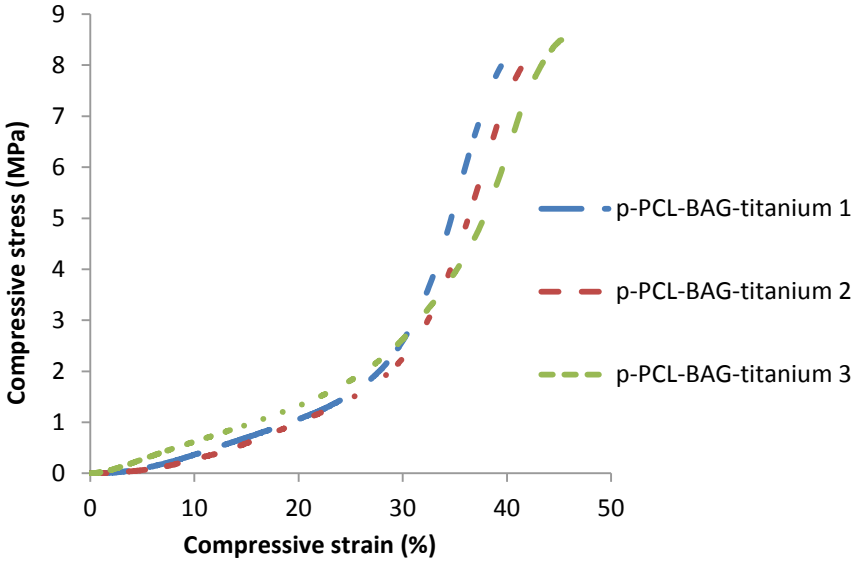

Figure 42. Compression stress-strain curves for p-PCL-BAG-titanium samples.

Figure 43 shows compression stresses at break for samples containing titanium. The 95-% confidence borders are determined for titanium and p-PCL-BAG-titanium samples. For the titanium-bone sample, confidence borders are not determined because only one sample was tested.

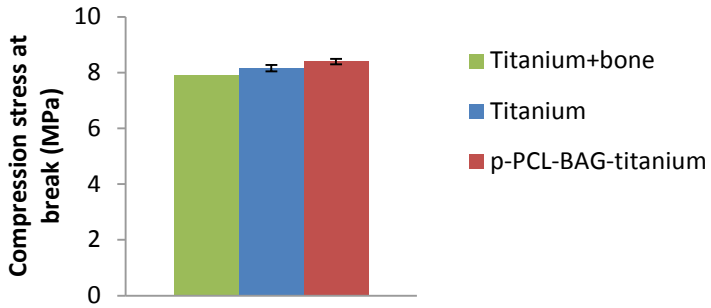

Figure 43. Compression stresses at break with 95-% confidence borders.

Figure 44 shows the compression stress-strain curves for porous PCL samples (p-PCL). Compression stress at break is significantly lower compared to all the other compression samples. Therefore, the porous PCL matrix in titanium mesh does not effect on the compression stress at break. This fact can be also seen comparing Figure 41 and Figure 42. The values show also that porous PCL could not be used without reinforcing titanium in any load-bearing application.

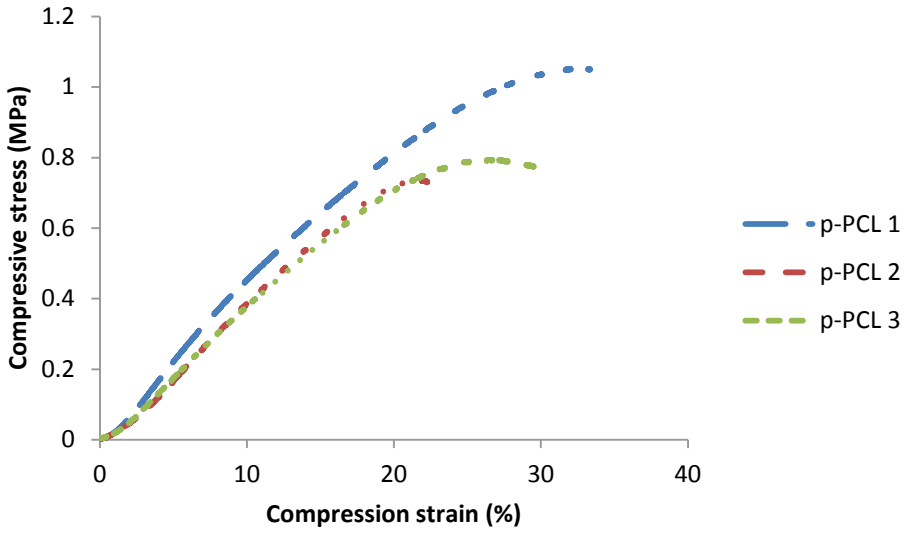

Figure 44. Compression stress-strain curves for p-PCL samples.

The non-porous PCL and PCL-BAG samples have the highest compression stresses at break (Figure 45 and Figure 46). The breaking of the samples starts at one side by cleavage of a piece, and continues by a small piece at a time.

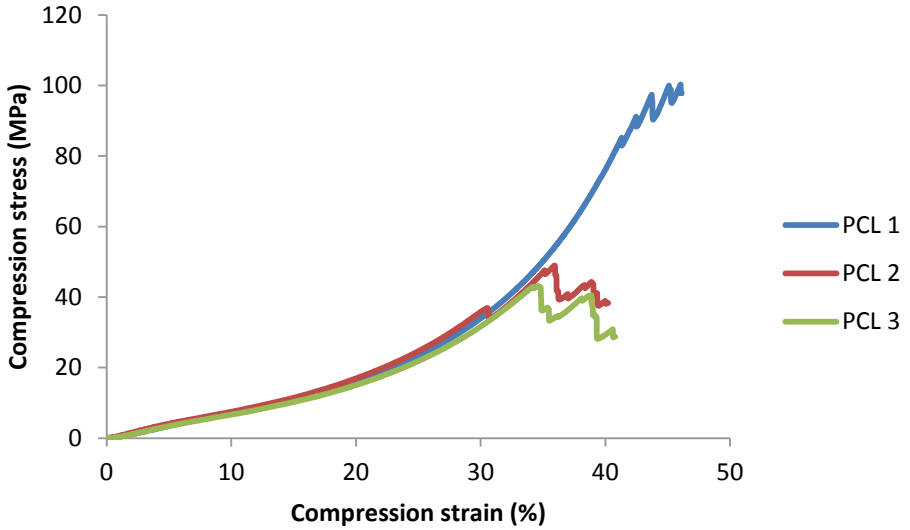

Figure 45. Compression stress-strain curves for PCL samples.

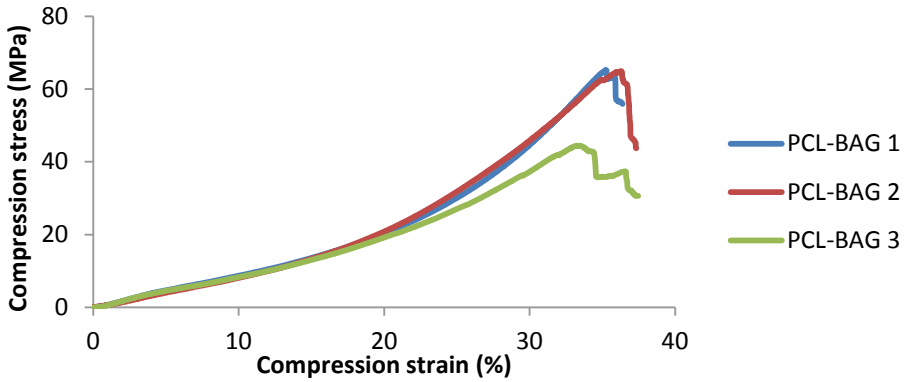

Figure 46. Compression stress-strain curves for PCL-BAG samples.

Trabecular bone samples had been stored at 80 % ethanol in refrigerator. Before testing the samples were in the testing environment for 1 h. There were two samples: the first one was from the femoral head and the second one from the femoral neck. The femoral neck sample was a lot more porous from other end. The difference in porosity can be seen in compressive strength at break in Figure 47.

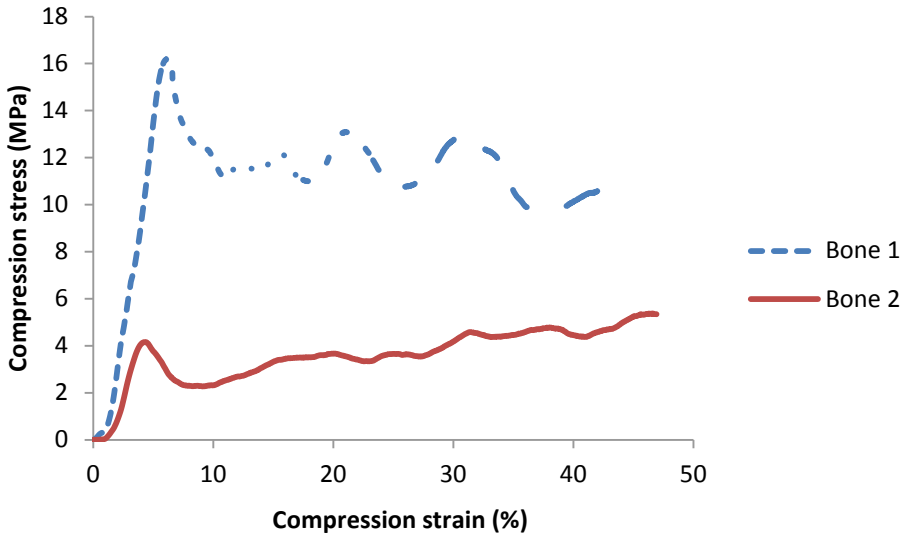

Figure 47. Compression stress-strain curves for trabecular bone samples. Bone 1: Femoral head. Bone 2: Femoral neck.

The modulus of elasticity is also important factor in mechanical behavior. The stress shielding occurs when a scaffold is much stronger than bone [8]. Therefore, it is an advantage that the value of modulus of elasticity of the material is close to that of bone. The literature values for trabecular bone are 0.02-1.9 GPa. [12] Figure 48 shows compressive modulus values for all samples. The confidence borders for bone samples have not been calculated because there was only one specimen of each sample containing bone. As seen in Figure 48, the compressive modulus values for titanium meshes are close to those of trabecular bone. The sample p-PCL-BAG-titanium is exception. This is due to the porous polymer around the titanium mesh.

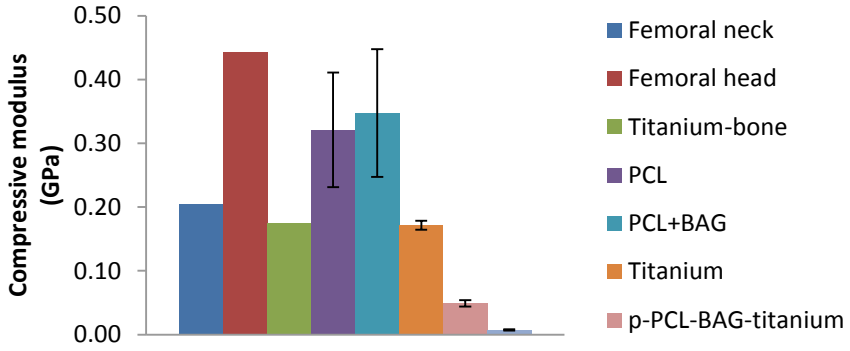

Figure 48. Compressive modulus with 95-% confidence borders for all the compressive samples.

The formability of Ti64 mesh after EBM manufacturing has been a subject of interest. Therefore, a set of experiments was made. As the titanium mesh starts to break after 9.5 % strain, it is interesting to see if the deformation reversible with lower strain. The titanium meshes were compressed so that the strain was 2 %, 4 %, 6 %, 8 % and 10 %. 2 % strain corresponds 0.3 mm strain. The sample height was measured before and immediately after the compression test. The height was also measured 12 hours after compression test to determine whether the deformation was reversible or irreversible.

The measurements showed that deformation was reversible with 2 and 4 % strains. 6 % strain yielded small, under 0.04 mm deformation. 8 % strain (1.2 mm) yielded deformation of 0.3 mm and 10 % 0.6 mm. When the strain was 10 %, the first breakage of titanium strut had happened. This affects already to the compression strength of titanium mesh. Therefore, the possible deformation is very small. To conclude, Ti64 mesh should not be deformed because the possible deformation is small and there is a great risk of breaking the struts.

10.5 Scanning electron microscope images

The scanning electron microscope (SEM) images were taken at Aalto University Nano-talo with Sigma VP (Zeiss, Germany). Emitech K100X (Quorum Technologies Ltd., United Kingdom) was used to coat samples with Gold/Palladium sputtering. The coating was performed with 30 mA coating current for 2 min. The titanium mesh does not require sputtering. The imaged samples were EBM manufactured titanium mesh, bioactive glass powder and two freeze extraction manufactured samples (PCL and PCL+BAG).

Figure 49 shows the surface of titanium mesh. EBM uses titanium powder and supposedly these powder particles are still seen on the surface of the mesh. The particle size is approximately 9 µm. The rough surface of EBM manufactured titanium mesh may be benefit for adhesion of osteogenic cells [47].

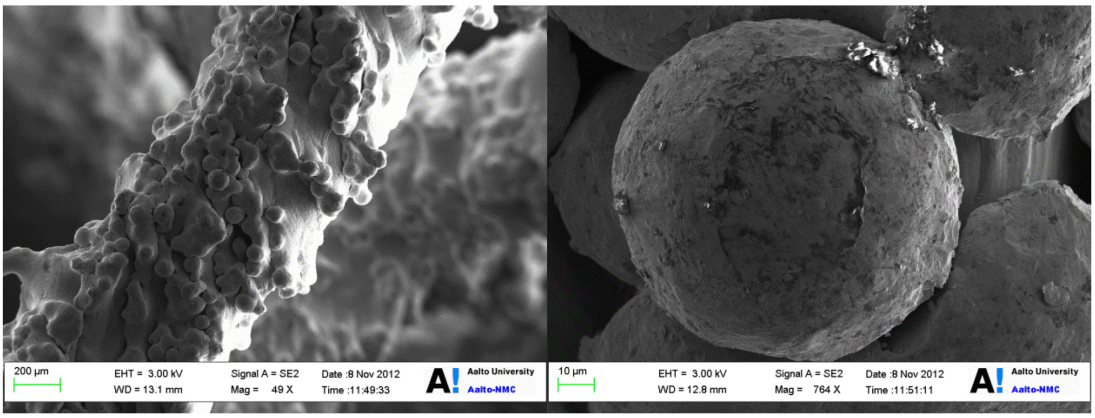

Figure 49. SEM images of EBM manufactured titanium mesh.

Figure 50 shows SEM images of bioactive glass (BAG) powder. This BAG was used also in the freeze extraction sample and PCL samples prepared from photo-crosslinkable oligomers. As shown in the images, the particle size of the BAG powder was not uniform, but rather distributed.

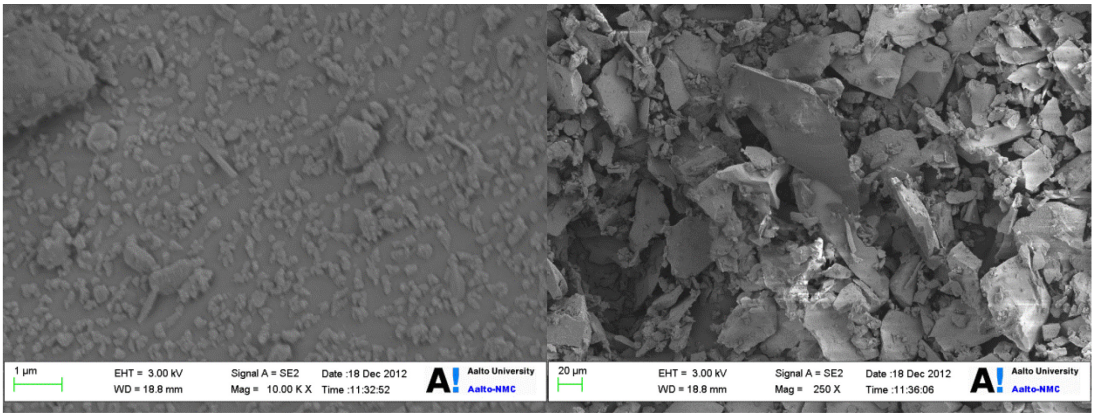

Figure 50. SEM images of bioactive glass (S53P4).

Figure 51 and Figure 52 show vertical and horizontal cross-sections of PCL and PCL-BAG samples prepared by freeze extraction. The Teflon mold has directed the evaporation of 1,4-dioxane and alignment of pores has been formed. The pores are ≥ 30 µm. There is no remarkable difference between the two samples. Furthermore, similar particles as seen in Figure 50 of bioactive glass cannot be seen in Figure 52.

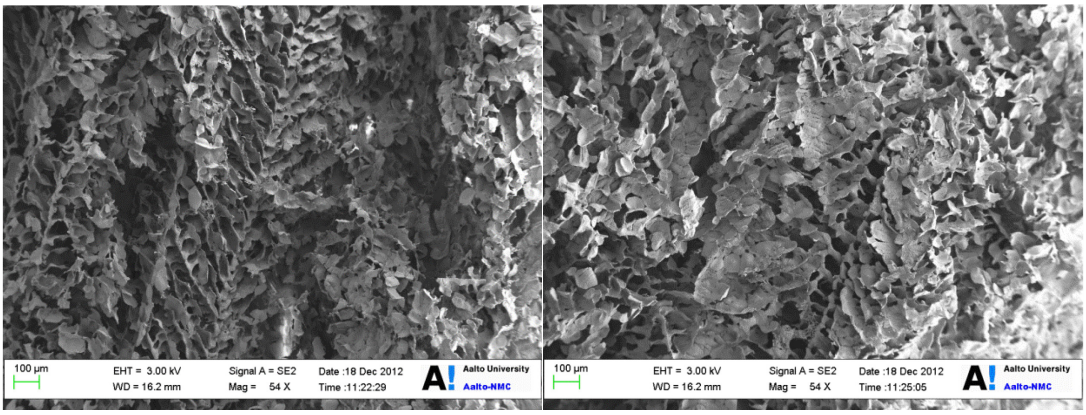

Figure 51. SEM image of PCL sample prepared by freeze extraction. Vertical (left) and horizontal (right) cross-section.

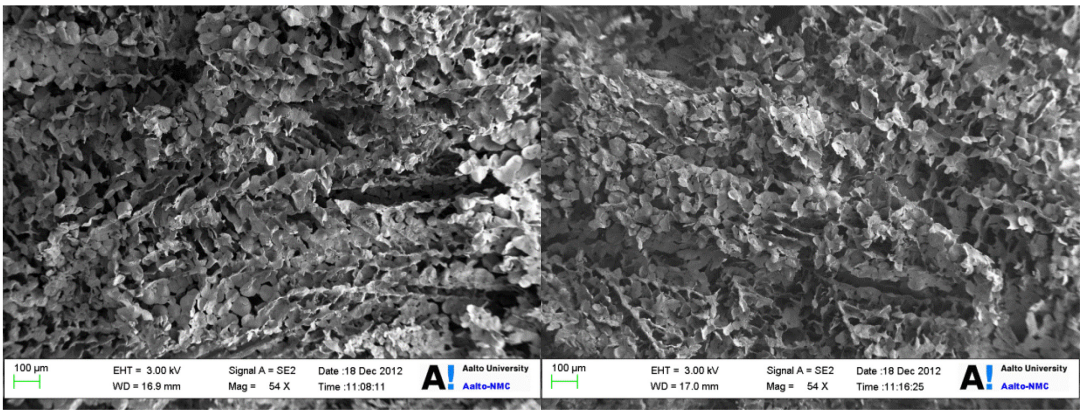

Figure 52. SEM image of PCL-BAG sample prepared by freeze extraction. Vertical (left) and horizontal (right) cross-section.

10.6 Micro-computed tomography

Micro-computed tomography (µCT) imaging was carried out at University of Oulu with SkyScan1176 high resolution in-vivo x-ray microtomograph. The SkyScan 1176 is used at preclinical research. The imaging shows that bone fills the mesh quite evenly. Figure 53 shows section of titanium mesh filled with crushed bone. During filling, few titanium particles have been pulled away from the mesh as can be seen in the Figure 53. Analysis of data reveals bone and tissue volumes in the sample. The percent of bone volume is 22 % and the percent of titanium volume is 7 %. Therefore, the total volume of titanium and bone is 29 % and the void space is 71 %.

The amount of void space can be reduced by using crushed bone graft with smaller particle size.

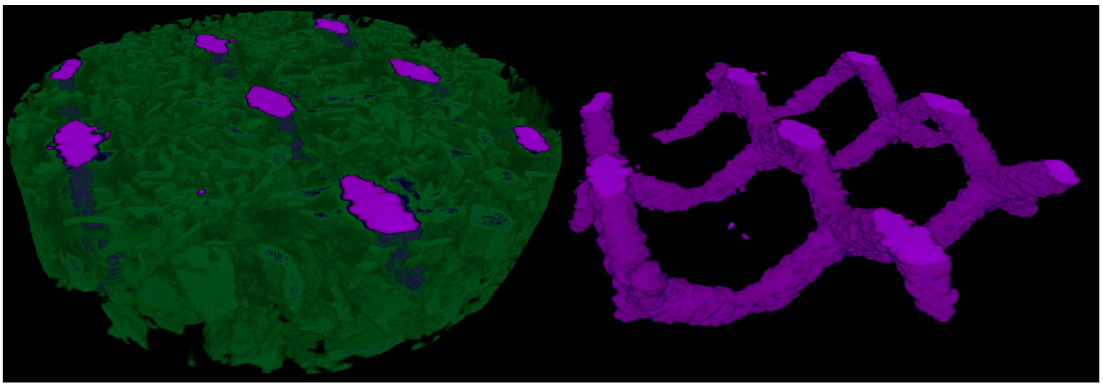

Figure 53. µCT image of titanium-bone sample. Titanium is purple and bone green.

Figures 54 and 55 show µCT images of PCL and PCL-BAG samples prepared by freeze extraction, respectively. µCT images reveal large voids that can be clearly seen in the middle of the samples. The presentage of total porosity volume was 66 % with PCL sample. The closed porosity was under 0.05 %. Therefore, most of the pores were interconnected. The pore alignment is clearer in PCL sample compared to PCL-BAG sample.

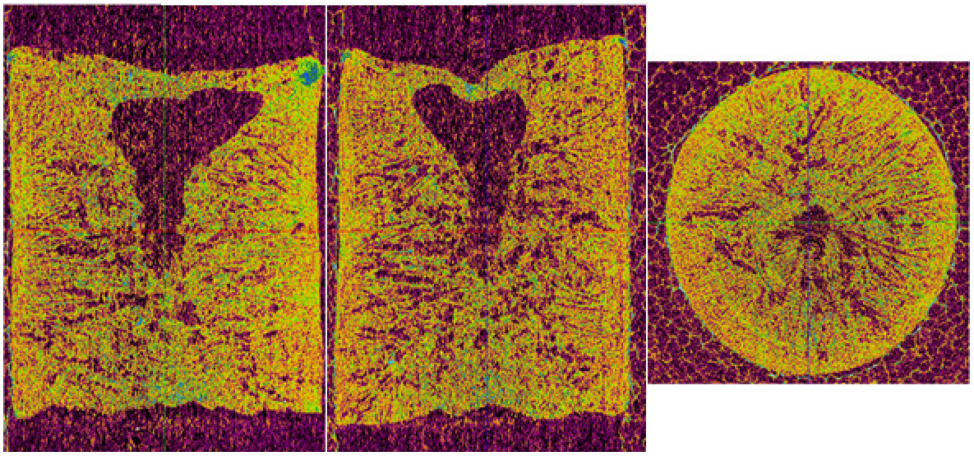

Figure 54. µCT images of PCL sample prepared by freeze-extraction. PCL is yellow and voids are purple.

Figure 55 reveals that bioactive glass has sunk to the bottom of the sample. This is probably due to a too slow freezing of the sample which gives BAG time to sink. The

volume percent of PCL was 18 % and BAG 8 %. Therefore, the porosity was 74 %. The volume percent of BAG of polymer matrix was 34 %.

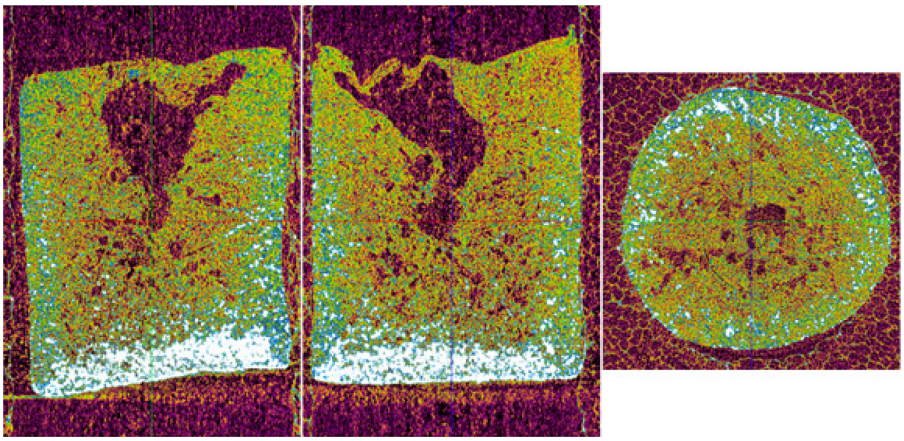

Figure 55. µCT images of PCL-BAG sample prepared by freeze-extraction. PCL is yellow, bioactive glass is white and voids are purple.

10.7 Cone beam computed tomography

Cone beam computed tomography (CBCT) imaging was carried out at University of Oulu with Planmed Verity® Extremity CT Scanner (Planmed Oy, Finland). The Planmed Verity® is developed for orthopedic imaging of patients and it provides high resolution 3D images. CBCT images were taken of titanium alloys mesh filled with crushed bone (Figure 56).

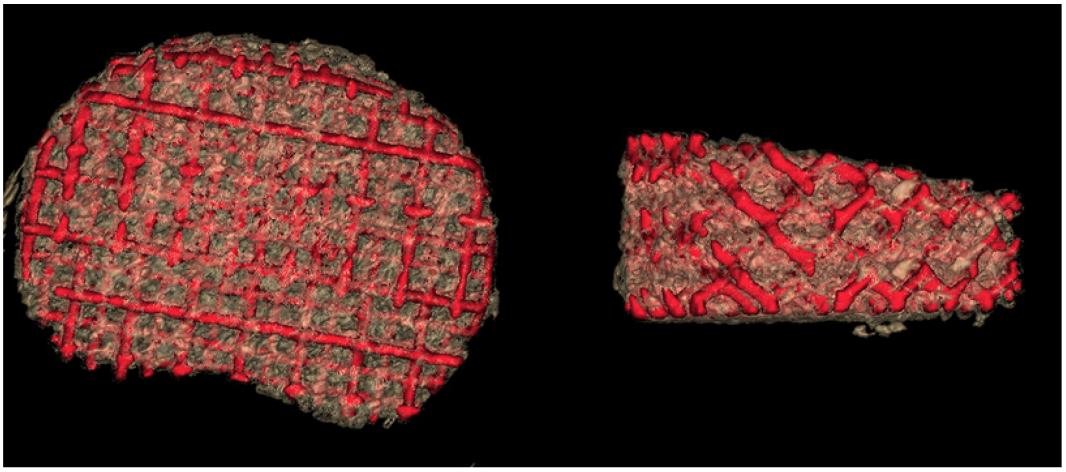

Figure 56. CBCT images of titanium-bone sample. Titanium mesh is colored red.

CBCT allows the studying different components of sample. One component can be faded out and other component can be viewed. Figure 57 shows a titanium/bone graft sample in which the bone graft is faded out.

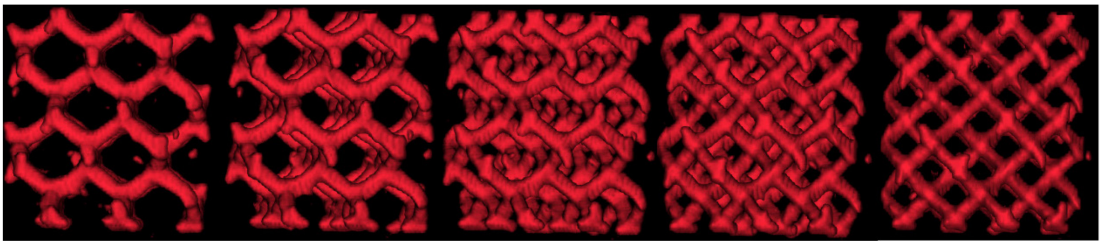

Figure 57. CBBT image of circular titanium mesh at different angles.

11 Conclusions

The target of this thesis was to manufacture 3D porous bioactive load-bearing hybrid material. The primary material choice was to combine titanium mesh with a biodegradable polymer. Bioactivity was obtained by using bioactive glass or bone graft. However, in this thesis the bioactivity was not tested with a cell cultivation experiment. On the other hand, bioactive glass is widely known to induce osteogenesis. Secondly, also the use of crushed bone graft as a titanium mesh filler was investigated. Bone graft is a naturally bioactive material which has already been used in several cage applications

The pore size in orthopedic implants should be 200-600 µm to allow bone ingrowth [27]. The favorable porosity of biomaterials is 60-70 % [78]. The pore size of EBM manufactured Ti64 mesh was 4 mm and porosity was 94 % because the mesh was planned to be filled with biodegradable polymer with a suitable porosity. The porosity of the freeze extraction sample was 66 % and the porous structure was interconnected as the µCT imaging showed. However, the pores were probably too small (≤ 30 µm) for osteoblasts as seen in SEM images. Therefore, the freeze extraction method should be improved concerning the pore size if there is a wish to use it in preparing a scaffold material. The µCT images also revealed that the BAG sunk to the bottom of the sample. Therefore, fast freezing is remarkably important for the even distribution of BAG in polymer matrix.

Porosity of photocrosslinkable polymers (56 %) was obtained by the salt leaching method. All of the salt was not possible to be removed from polymer matrix which was noticed by weighting the samples. Salt leaching with $CaCl_2 \cdot 6\ H_2O$ is not probably suitable method for samples of this size. Another possibility might be that the sieving $CaCl_2 \cdot 6\ H_2O$ with 0.5 mm sieve used in this study does not yield optimal salt particle size for the method. Salt leaching with $CaCl_2 \cdot 6\ H_2O$ has been reported to yield pore size 220 ± 80 µm [78]. The gel content inside the cross-linked PCL samples was high. This proves that in case of clear samples, good photocrosslinking is possible to obtain with larger samples. However, the shading effect of bioactive glass or titanium mesh to photocrosslinking is not known.

EBM manufactured titanium meshes had compressive stress at break approximately 8 MPa at 9.5 % strain and compressive modulus 0.17 GPa. These values are close to the values of trabecular bone, of which compression stress is 2-22 MPa and

elastic modulus 0.02-1.19 GPa depending on the source. Also the trabecular bone samples measured had a similar compressive stress at break (4 and 16 MPa) and compressive modules (0.21 and 0.44 GPa). Therefore, titanium mesh might be suitable for load-bearing applications in replacing trabecular bone. In addition, at least one implant consisting EBM manufactured Ti64 alloy has got FDA approval. There are also several CE-certified and FDA-cleared implants on the market produced according to the EBM manufacturer Arcam AB [84]. To conclude, EBM manufactured titanium mesh is an attractive option as a bone implant material.

12 Suggestion for future work

First of all, the design of an implant should be considered carefully. The overall structure of titanium mesh needs evaluation. The roughness of titanium surface can be seen as an advantage but also as a demerit. The surface roughness gives a tight fit with vertebrae. On the other hand, the rough surface makes it more difficult to get the implant between the vertebrae, especially when the space between the vertebrae is very small. Screws to assist the fixation of the implant might be needed to avoid slip. Therefore, designing places for screws would be an option for further development. Now the focus has been on preparing interbody cages. One option could also be to prepare longer vertebral body replacements. Those are needed in situations, where one or more vertebrae have to be removed, such as in cancer.

As cited earlier, it is profitable that spinal implant patients receive antibiotics in connection with surgery [61]. Therefore, when a biodegradable polymer is used, antibiotics could be added in polymer matrix. This would create a drug release device. There is also an option to grow bone cells into the scaffold before implantation, which creates an osteogenic implant.

Mechanical properties of hybrid materials need revising. Titanium mesh has now had a compression strength at break similar to trabecular bone values in literature. However, as spine has a complex mechanical environment, other mechanical testing would be profitable, such as shear and bending testing. Fatigue testing has shown that EBM manufactured Ti64 mesh is not optimal for applications with cyclic load. [20] Therefore, the Ti64 mesh might not be the optimal material in spine.

Relative density has effect on compressive strength of EBM meshes [12]. Therefore, through increasing the relative density, it would be possible to prepare titanium networks with a higher compressive strength. This would allow the use of titanium mesh scaffolds in cortical bone. On the other hand, the application area could also be in environment where load-bearing property is not essential, such as fundus implant.

Bioactivity has now been proposed to yield from bioactive glass in biodegradable polymer matrix or crushed bone graft. The path should now be decided; the choice will affect the design of titanium mesh. With bone graft the design should help maintaining the bone graft inside the titanium mesh. If the use of biodegradable

polymer would be the choice, the porosity should be optimized. Salt leaching might not be the best solution due to the remaining salt in the matrix. As freeze extraction produces too small pores and freeze drying did not succeed, some method to prepare porous polymer matrix inside the titanium mesh should be found.

The porous structure of freeze extraction and drying methods is formed during the freezing state. Therefore, suggestions to improve freeze extraction and freeze drying methods are partly similar. For example, water has been noticed to effect on porous structure of PLLA dissolved in dioxane/water binary mixture [83].

The gel content with photocrosslinkable PCL samples was high. The gel content of samples with titanium or BAG was not determined because it is difficult with titanium samples and the test method is not valid with fillers. Therefore, to make sure that the crosslinking is high, there is a possibility to use a dual initiator, which initiates the crosslinking due both light and temperature.

Also the resorption rate of polymer in the body should be investigated, because one of the aims in biodegradable implants is to match the resorption rate with the cell growth rate. In addition to PCL, other biodegradable polymers should be considered because polymers have different resorption rates. It is also possible to adjust the resorption rate by using copolymers.

When there is a decision about implant materials, the next step in the research would be cell cultivation test. The bioactivity of the implant should be tested. If the cell cultivation tests are promising, experimental study with animals should be considered.

13 References

[1] Pruitt, L.A., Chakravartula, A.M., *Mechanics of Biomaterials - Fundamental Principles for Implant Design*, Cambridge University Press, Cambridge 2011, pp. 644.

[2] Geetha, M., Singh, A.K., Asokamani, R., Gogia, A.K. Ti Based Biomaterials, the Ultimate Choice for Orthopaedic Implants – A Review, *Progress in Materials Science* **54** (2009) 397-425.

[3] Tortora, G.J., Grabowski, S.R., *Principles of Anatomy and Physiology*, 9th ed., John Wiley & Sons, New York 2000, pp. 1055.

[4] Deng, H., Liu, Y., *Current Topics in Bone Biology*, World Scientific, Hackensack NJ 2005 pp. 540.

[5] Hench, L.L., Jones, J.R., *Biomaterials, Artificial Organs and Tissue Engineering*, Woodhead publishing, Boston 2005, pp. 308.

[6] Karageorgiou, V., Kaplan, D., Porosity of 3D Biomaterial Scaffolds and Osteogenesis. Biomaterials **26 (**2005) 5474-5491.

[7] Black, J., Hastings, G., *Handbook of Biomaterial Properties*, Springer - Verlag , London 1998, pp. 629.

[8] Buschow, K.H.J., *Encyclopedia of Materials: Science and Technology*., Elsevier: Amsterdam 2001, pp. 12066.

[9] Oh, I.-., Nomura, N., Masahashi, N., Hanada, S., Mechanical Properties of Porous Titanium Compacts Prepared by Powder Sintering. *Scr. Mater*. **49** (2003) 1197-1202.

[10] Nakai, M., Niinomi, M., Akahori, T., Tsutsumi, H., Itsuno, S., Haraguchi, N., Itoh, Y., Ogasawara, T., Onishi, T., Shindoh, T., Development of Biomedical Porous Titanium Filled with Medical Polymer by in-Situ Polymerization of Monomer Solution Infiltrated into Pores, *Journal of the Mechanical Behavior of Biomedical Materials* **3** (2010) 41-50.

[11] Niinomi, M., Mechanical Biocompatibilities of Titanium Alloys for Biomedical Applications, *Journal of the Mechanical Behavior of Biomedical Materials* **1** (2008) 30-42.

[12] Heinl, P., Körner, C., Singer, R., Selective Electron Beam Melting of Cellular Titanium: Mechanical Properties, *Advanced Engineering Materials* **10** (2008) 882-888.

[13] Kamachi Mudali, U., Sridhar, T.M., Baldev, R.A.J., Corrosion of Bio Implants, *Sadhana - Academy Proceedings in Engineering Sciences* **28** (2003) 601-637.

[14] Williams, D.F., On the Nature of Biomaterials, *Biomaterials* **30** (2009) 5897-5909.

[15] Ratner, B.D., Hoffman, A.S., Schoen, F.J., Lemons, J.E., *Biomaterials Science an Introduction to Materials in Medicine*, 2nd ed., Elsevier Academic Press, San Diego, California 2004, pp. 851.

[16] Williams, D.F., On the Mechanisms of Biocompatibility, *Biomaterials* **29** (2008) 2941-2953.

[17] Khan, W.S., Rayan, F., Dhinsa, B.S., Marsh, D., An Osteoconductive, Osteoinductive, and Osteogenic Tissue-Engineered Product for Trauma and Orthopaedic Surgery: How Far are we?, *Stem Cells International* (2012) 1-7.

[18] Blokhuis, T.J., Arts, J.J.C., Bioactive and Osteoinductive Bone Graft Substitutes: Definitions, Facts and Myths. *Injury* **42** (2011) S26-S29.

[19] Groeneveld, E.H.J., Van Den Bergh, J.P.A., Holzmann, P., Ten Bruggenkate, C.M., Tuinzing, D.B., Burger, E.H. Mineralization Processes in Demineralized Bone Matrix Grafts in Human Maxillary Sinus Floor Elevations. *J. Biomed. Mater. Res.* **48** (1999) 393-402.

[20] Hrabe, N.W., Heinl, P., Flinn, B., Körner, C., Bordia, R.K., Compression-Compression Fatigue of Selective Electron Beam Melted Cellular Titanium (Ti-6Al-4V), *Journal of Biomedical Materials Research - Part B Applied Biomaterials* **99** (2011) 313-320.

[21] Cheng, X.Y., Li, S.J., Murr, L.E., Zhang, Z.B., Hao, Y.L., Yang, R., Medina, F., Wicker, R.B., Compression Deformation Behavior of Ti-6Al-4V Alloy with Cellular Structures Fabricated by Electron Beam Melting, *Journal of the Mechanical Behavior of Biomedical Materials* **16** (2012) 153–162.

[22] Sumitomo, N., Noritake, K., Hattori, T., Morikawa, K., Niwa, S., Sato, K., Niinomi, M., Experiment Study on Fracture Fixation with Low Rigidity Titanium Alloy: Plate Fixation of Tibia Fracture Model in Rabbit. *J. Mater. Sci. Mater. Med.,* **19** (2008) 1581-1586.

[23] Rubstein, A.P., Makarova, E.B., Trakhtenberg, I.S., Kudryavtseva, I.P., Bliznets, D.G., Philippov, Y.I., Shlykov, I.L., Osseointegration of Porous Titanium Modified by Diamond-Like Carbon and Carbon Nitride, *Diamond and Related Materials* 22 **(2012)** 128-135.

[24] Barbas, A., Bonnet, A., Lipinski, P., Pesci, R., Dubois, G., Development and Mechanical Characterization of Porous Titanium Bone Substitutes, *Journal of the Mechanical Behavior of Biomedical Materials* **9** (2012) 34-44.

[25] Kuboki, Y., Takita, H.; Kobayashi, D., Tsuruga, E., Inoue, M., Murata, M., Nagai, N., Dohi, Y., Ohgushi, H., BMP-Induced Osteogenesis on the Surface of Hydroxyapatite with Geometrically Feasible and Nonfeasible Structures: Topology of Osteogenesis, *J. Biomed. Mater. Res.* **39** (1998) 190-199.

[26] Teixeira, L.N., Crippa, G.E., Lefebvre, L., De Oliveira, P.T., Rosa, A.L., Beloti, M.M., The Influence of Pore Size on Osteoblast Phenotype Expression in Cultures Grown on Porous Titanium, *Int. J. Oral Maxillofac. Surg.* **41** (2012) 1097-1101.

[27] Li, X., Feng, Y., Wang, C., Li, G., Lei, W., Zhang, Z., Wang, L., Evaluation of Biological Properties of Electron Beam Melted Ti6Al4V Implant with Biomimetic Coating in Vitro and in Vivo, *PLoS ONE* **7** (2012).

[28] Chu, T., Orton, D.G., Hollister, S.J., Feinberg, S.E., Halloran, J.W., Mechanical and in Vivo Performance of Hydroxyapatite Implants with Controlled Architectures, *Biomaterials* **23** (2002) 1283-1293.

[29] Daintith, J.,Martin, E. , Dictionary of Science, 6th Ed., Oxford University Press, Oxford 2010, pp. 900.

[30] Cao, W., Hench, L.L., Bioactive Materials. *Ceram. Int.* **22** (1996) 493-507.

[31] Lindfors, N.C., Aho, A.J., Tissue Response to Bioactive Glass and Autogenous Bone in the Rabbit Spine, *European Spine Journal* **9** (2000) 30-35.

[32] Jain, J.P., Yenet Ayen, W., Domb, A.J., Kumar, N., Biodegradable Polymers in Drug Delivery, In *Biodegradable Polymers in Clinical use and Clinical Development*., edited by Domb, A., Kumar, N., Ezra, A., John Wiley & Sons, Inc., 2011, pp. 1-58.

[33] Woodruff, M.A., Hutmacher, D.W., The Return of a Forgotten Polymer - Polycaprolactone in the 21st Century, *Progress in Polymer Science* **35** (2010) 1217-1256.

[34] Gu, D.D., Meiners, W., Wissenbach, K., Poprawe, R., Laser Additive Manufacturing of Metallic Components: Materials, Processes and Mechanisms, *International Materials Reviews* **57** (2012) 133-164.

[35] Müller, U., Imwinkelried, T., Horst, M., Sievers, M., Graf-Hausner, U. Do Human Osteoblasts Grow into Open-Porous Titanium?, *European Cells and Materials* **11 (2006)** 8-15.

[36] Palmquist, A., Snis, A., Emanuelsson, L., Browne, M., Thomsen, P., Long-Term Biocompatibility and Osseointegration of Electron Beam Melted, Free-Form-Fabricated Solid and Porous Titanium Alloy: Experimental Studies in Sheep, *J. Biomater. Appl.* (2011) 1-14.

[37] Torres, Y., Pavón, J.J., Rodríguez, J.A., Processing and Characterization of Porous Titanium for Implants by using NaCl as Space Holder, *J. Mater. Process. Technol.* **212** (2012) 1061-1069.

[38] Li, J.P., de Wijn, J.R., Van Blitterswijk, C.A., de Groot, K., Porous Ti6Al4V Scaffold Directly Fabricating by Rapid Prototyping: Preparation and in Vitro Experiment, *Biomaterials* **27** (2006) 1223-1235.

[39] Wen, C.E., Mabuchi, M., Yamada, Y., Shimojima, K., Chino, Y., Asahina, T., Processing of Biocompatible Porous Ti and Mg, *Scr. Mater.* **45 (2001)** 1147-1153.

[40] Lefebvre, L., Yannig, T., Method of Making Open Cell Material, Patent number 6660224, 2003.

[41] Palmer, R. The Knee Bone's Connected to the.. Titanium Foam?, *Nat. Med.* **16 (2010)** 1170.

[42] Peter Quadbeck, Fraunhofer, A., Titanium Foams Replace Injured Bones, http://www.fraunhofer.de/en/press/research-news/2010/09/titanium-foams-replace-injured-bones.html 24.8.2012.

[43] Heinl, P., Rottmair, A., Körner, C., Singer, R.F., Cellular Titanium by Selective Electron Beam Melting, *Advanced Engineering Materials* **9** (2007) 360-364.

[44] Murr, L.E., Esquivel, E.V., Quinones, S.A., Gaytan, S.M., Lopez, M.I., Martinez, E.Y., Medina, F., Hernandez, D.H., Martinez, E., Martinez, J.L., Microstructures and Mechanical Properties of Electron Beam-Rapid Manufactured Ti-6Al-4V Biomedical Prototypes Compared to Wrought Ti-6Al-4V, *Mater Charact* **60** (2009), 96-105.

[45] FIT-Production GmbH, A., Electron Beam Melting, http://www.fit-production.de/electron_beam_melting.php 20.9.2012.

[46] Ponader, S., Vairaktaris, E., Heinl, P., Wilmowsky, C.v., Rottmair, A., Körner, C., Singer, R.F., Holst, S., Schlegel, K.A., Neukam, F.W., Effects of Topographical Surface Modifications of Electron Beam Melted Ti-6Al-4V Titanium on Human Fetal Osteoblasts, *Journal of Biomedical Materials Research Part A* **84A** (2008) 1111-1119.

[47] Li, X., Luo, Y., Wang, C., Zhang, W., Li, Y., Fabrication and in Vivo Evaluation of Ti6Al4V Implants with Controlled Porous Structure and Complex Shape, *Frontiers of Mechanical Engineering* **7 (2012)** 66-71.

[48] Murr, L.E., Gaytan, S.M., Martinez, E., Medina, F., Wicker, R.B., Next Generation Orthopaedic Implants by Additive Manufacturing using Electron Beam Melting, *International Journal of Biomaterials* **2012** (2012) 1-14.

[49] Peter D. Rumm, FDA, Summary of Safety and Effectiveness, http://www.accessdata.fda.gov/cdrh_docs/pdf11/K112898.pdf, 24.1.2013.

[50] Limacorporate S.p.a, A., DELTA-ONE-TT, http://www.lima.it/product-delta_one_tt-5-10.html, 24.1.2013.

[51] Nakai, M., Niinomi, M., Ishii, D., Mechanical and Biodegradable Properties of Porous Titanium Filled with Poly-L-Lactic Acid by Modified in Situ Polymerization Technique, *Journal of the Mechanical Behavior of Biomedical Materials* **4** (2011) 1206-1218.

[52] Wang, J.F., Liu, X.Y., Luan, B., Fabrication of Ti/Polymer Biocomposites for Load-Bearing Implant Applications, *J. Mater. Process. Technol*. **197** (2008) 428-433.

[53] Niinomi, M., Nakai, M., Akahori, T., Tsutsumi, H., Yamanoi, H., Itsuno, S., Haraguchi, N., Itoh, Y., Ogasawara, T., Onishi, T., Functionality of Porous Titanium Improved by Biopolymer Filling, *Ceramic Transactions* **206** (2009) 91-101.

[54] Watanabe, Y., Iwasa, Y., Sato, H., Teramoto, A., Abe, K., Miura-Fujiwara, E., Microstructures and Mechanical Properties of Titanium/Biodegradable-Polymer FGM for Bone Tissue Fabricated by Spark Plasma Sintering Method, *J. Mater. Process. Technol.* **211** (2011) 1919-1926.

[55] Vrana, N.E., Dupret, A., Coraux, C., Vautier, D., Debry, C., Lavalle, P., Hybrid Titanium/Biodegradable Polymer Implants with an Hierarchical Pore Structure as a Means to Control Selective Cell Movement. PLoS ONE **6** (2011).

[56] Serro, A.P., Saramago, B., Influence of Sterilization on the Mineralization of Titanium Implants Induced by Incubation in various Biological Model Fluids, *Biomaterials* **24 (2003)** 4749-4760.

[57] Lewis, G., Nucleus Pulposus Replacement and Regeneration/Repair Technologies: Present Status and Future Prospects, *Journal of Biomedical Materials Research - Part B Applied Biomaterials* **100B** (2012) 1702-1720.

[58] Van Den Eerenbeemt, K.D., Ostelo, R.W., Van Royen, B.J., Peul, W.C., Van Tulder, M.W., Total Disc Replacement Surgery for Symptomatic Degenerative Lumbar Disc Disease: A Systematic Review of the Literature, *European Spine Journal* **19** (2010) 1262-1280.

[59] Chan, S.C.W., Gantenbein-Ritter, B., Intervertebral Disc Regeneration Or Repair with Biomaterials and Stem Cell Therapy - Feasible Or Fiction? *Swiss Medical Weekly* **142** (2012).

[60] Gerometta, A., Rodriguez Olaverri, J.C., Bittan, F., Infection and Revision Strategies in Total Disc Arthroplasty. *Int. Orthop.* **36** (2012) 471-474.

[61] Quaile, A. Infections Associated with Spinal Implants., *Int. Orthop.* **36 (2012)** 451-456.

[62] Thalgott, J.S., Giuffre, J.M., Klezl, Z., Timlin, M., Anterior Lumbar Interbody Fusion with Titanium Mesh Cages, Coralline Hydroxyapatite, and Demineralized Bone Matrix as Part of a Circumferential Fusion, *The Spine Journal* **2** (2002) 63-69.

[63] Serhan, H., Mhatre, D., Defossez, H., Bono, C.M., Motion-Preserving Technologies for Degenerative Lumbar Spine: The Past, Present, and Future Horizons, *SAS Journal* **5 (2011)** 75-89.

[64] Omeis, I., DeMattia, J.A., Hillard, V.H., Murali, R., Das, K., History of Instrumentation for Stabilization of the Subaxial Cervical Spine, *Neurosurgical focus* 16 (2004).

[65] Van De Kelft, E., Verguts, L., Clinical Outcome of Monosegmental Total Disc Replacement for Lumbar Disc Disease with Ball-and-Socket Prosthesis (Maverick): Prospective Study with Four-Year Follow-Up, *World Neurosurgery* **78** (2012) 355-363.

[66] Wang, M.Y. Metal-on-Metal Lumbar Total Disc Arthroplasty: Ready for Prime Time?, *World Neurosurgery* **78** (2012) 247.

[67] Gamradt, S.C., Wang, J.C., Lumbar Disc Arthroplasty, *The Spine Journal* **5** (2005) 95-103.

[68] Zigler, J., Total Disc Replacement - ProDisc, http://www.spine-health.com/treatment/artificial-disc-replacement/total-disc-replacement-prodisc, 24.1.2013.

[69] Peloza, J.H., Lumbar Total Disk Replacement, http://www.centerforspinecare.com/approach/minimalinvasive/lowerback/realities.html, 24.1.2013.

[70] Anonymous, The Next Generation Interbody Fusion Devices, http://www.titanspine.com/content/products/overview.htm, 24.1.2013

[71] Anonymous, Trabecular Metal™ Material http://www.zimmer.co.uk/z/ctl/op/global/action/1/id/10003/template/MP/prcat/M6/prod/y#_TM_-_A:_Trabecular%20Metal%20ALIF%20Devic, 24.1.2013.

[72] Anonymous, Vertebral Spacers, http://www.synthes.com/sites/NA/Products/Spine/Interbody_and_Vertebral_Body_Replacement_Systems/Pages/Vertebral-Spacers.aspx, 24.1.2013.

[73] Anonymous, ORIO-AL ALIF PEEK-Optima® Cage, http://www.spinecraft.us/Products/Lumbar-Degenerative_6/ORIO-AL-ALIF-PEEK-Optima%C2%AE-Cage_15, 24.1.2013.

[74] Anonymous, PEEK Cage, http://bmkmedi.en.ec21.com/offer_detail/Sell_ALIF_PEEK_Cage--13212547.html?gubun=S 24.1.2013.

[75] Lange, U., Edeling, S., Knop, C., Bastian, L., Oeser, M., Krettek, C., Blauth, M., Anterior Vertebral Body Replacement with a Titanium Implant of Adjustable Height: A Prospective Clinical Study, *European Spine Journal* **16** (2007) 161-172.

[76] Knop, C., Lange, U., Bastian, L., Oeser, M., Blauth, M., Biomechanical Compression Tests with a New Implant for Thoracolumbar Vertebral Body Replacement, *European Spine Journal* **10** (2001) 30-37.

[77] Robertson, P.A.,Coldham, G.J., Anterior Surgery for Thoracolumbar Burst Fractures: Rationale and Technique, http://www.spineuniverse.com/professional/research/pathology/vascular/anterior-surgery-thoracolumbar-burst-fractures-rationale, 24.1.2013.

[78] Meretoja, V.V., Malin, M., Seppälä, J.V., Närhi, T.O., Osteoblast Response to Continuous Phase Macroporous Scaffolds Under Static and Dynamic Culture Conditions, *Journal of Biomedical Materials Research - Part A* **89** (2009) 317-325.

[79] Korhonen, H., Helminen, A., Seppälä, J.V., Synthesis of Polylactides in the Presence of Co-Initiators with Different Numbers of Hydroxyl Groups, *Polymer* **42** (2001) 7541-7549.

[80] Helminen, A.O., Korhonen, H., Seppälä, J.V., Structure Modification and Crosslinking of Methacrylated Polylactide Oligomers, *J Appl Polym Sci* **86** (2002) 3616-3624.

[81] Lebourg, M., Antón, J.S., Ribelles, J.L.G., Porous Membranes of PLLA-PCL Blend for Tissue Engineering Applications, *European Polymer Journal* **44 (2008)** 2207-2218.

[82] Gaona, L.A., Gómez Ribelles, J.L., Perilla, J.E., Lebourg, M., Hydrolytic Degradation of PLLA/PCL Microporous Membranes Prepared by Freeze Extraction, *Polym. Degrad. Stab.* **97 (2012)** 1621-1632.

[83] Ho, M., Kuo, P., Hsieh, H., Hsien, T., Hou, L., Lai, J., Wang, D., Preparation of Porous Scaffolds by using Freeze-Extraction and Freeze-Gelation Methods, *Biomaterials* **25 (2004)** 129-138.

[84] Anonymous, Medical implants, http://www.arcam.com/industry-segments/medical-implants.aspx, 24.1.2013.